The Synthesis of Phosphonic Acid-Functionalized Polymeric Spherical Particles by Heterogeneous Polymerization Method and Their Adsorption Properties of Metal Ions

(不均一重合法によるホスホン酸官能化高分子球状粒子の合成とそれらの金属イオンの吸着特性)

BENNY RIO FERNANDEZ

Doctor of Philosophy

Department of Chemistry
Graduate School of Science
Osaka University
2022

Doctoral Dissertation

The Synthesis of Phosphonic Acid-Functionalized Polymeric Spherical Particles by Heterogeneous Polymerization Method and Their Adsorption Properties of Metal Ions

(不均一重合法によるホスホン酸官能化高分子球状粒子の合成とそれらの金属イオンの吸着特性)

by

BENNY RIO FERNANDEZ

Chief examiner:

Professor Satoshi TSUKAHARA

Second Readers:

Professor Takashi YOSHIMURA

Professor Motohiro NAKANO

Department of Chemistry, Graduate School of Science

Osaka University

2022

Acknowledgement

First and foremost, praises and thanks to the God, the Almighty, for His showers of blessings throughout my research work.

I would like to express my gratitude and appreciation to my supervisor Professor Satoshi TSUKAHARA, for giving me the opportunity to undertake this Ph.D study and for his valuable support and supervision. I am thankful to Professor Takashi YOSHIMURA and Professor Motohiro NAKANO for their valuable comments. I also would like to give special thanks to the Assistant Professor Dr. Masayori SUWA and Dr. Shigeki YAMAMOTO for sharing his expertise and for giving his time generously.

I would like to thank to all laboratory members for making enjoyable place to work and good atmospheric to study.

I would like to express my gratitude and love to my wife, who has always lovingly been by my side. Heartfelt thanks to my lovely kids RAFFASYA and FLAVA. Also, extremely grateful to my parents and my big family for their love, continued support, encouragement, and advice.

I wish to acknowledge and thank for the financial support from the Researcher Development Project in Basic Science, Monbukagakusho Honor Scholarship for Privately-Financed International Students from JASSO, and Matsuda Yosahichi Memorial Foreign Student Scholarship for the Ph.D course at Osaka University, Japan.

Finally, my thanks go to all the people who have supported me to complete the research work either directly or indirectly

March, 2022

Abstract

The heterogeneous polymerization is widely applied for producing a vast amount of polymeric particles, where emulsion and suspension polymerization are a part of such a process. As for its components, the emulsion method enables the production of oil-in-water (O/W), while the suspension method is possible to produce a water-in-oil (W/O) system. Surface-functionalized polymers have attracted widespread interest in many applications. Functionalization of polymers with functional desire groups, i.e., phosphonic acid group, are helpful in various fields such as catalyst, paint, and others.

This thesis focused on synthesizing phosphonic acid-functionalized polymeric spherical particles through either emulsion or suspension polymerization method. Obtained spherical polymer particles were applied to adsorb metal ions and study their adsorption kinetic properties.

Firstly, the synthesis of phosphonic acid-functionalized on styrene and divinylbenzene nanoparticles was successfully conducted by the O/W emulsion polymerization method. This method comprising two primary components, they are (1) the aqueous phase (water, water-soluble initiator, and functional agent) as the continuous phase and (2) the oil phase (monomer and crosslinker) as a droplet. All of the components are mixed under N_2 gas at 70^{o}C with a stirring process at 100 rpm. IR results reveal that phosphonic acid groups were successfully grafted onto polymer main chains. SEM image (**Fig.1a**) shows that the functionalized nanoparticles are uniform and spherical.

On the other hand, I also successfully synthesized the nanoparticle-based on styrene and divinylbenzene with a similar method. This non-functionalized polymer also shown high uniformity and spherical shape (**Fig.1b**).

Secondly, crosslinked poly(vinylphosphonic acid) particles were successfully synthesized using the W/O suspension polymerization method in the presence of vinylphosphonic acid as a monomer, poly(ethylene glycol) diacrylate (PEGDA) as a crosslinker, and Benzoyl peroxide (BPO) as an initiator. The PEGDA content was varied from 5% to 20 % molar ratio concerning VPA. In this term, the aqueous phase (monomer, crosslinker, stabilizer, and water) is a droplet, and the oil phase (silicone oil and oil-soluble initiator) is the continuous phase. Briefly, two separate mixtures are combined after thoroughly mixing in their respective phase under N_2 gas at 65^{o}C with a stirring process at 400 rpm. The obtained particles were characterized by IR spectroscopy, optical microscope, and SEM. The particles were polydisperse and spherical. Their sizes ranged from 10 to 200 μm, as shown in **Fig.2**.

In order to investigate the kinetic study on the adsorption, a batch adsorption experiment was employed to trivalent (Ln^{3+} = La^{3+}, Tb^{3+}, and Lu^{3+}) and divalent (Cu^{2+} and Zn^{2+}) metal ions. The adsorption kinetic study investigated the effect of PEGDA content, initial solution pH, contact time, and initial metal concentration to get the optimum conditions. In the preliminary study, the 10 % molar PEGDA (PVPA-10) ratio gave the highest adsorption capacity of Tb^{3+} ions than the others, and the adsorption was achieved at 60 min. Moreover, the adsorption of all metal ions was strongly pH-dependence due to the deprotonation of the phosphonic acid functional group on the adsorbent surface. We selected 5 x 10^{-5} mol L^{-1} as the optimum metal ions concentration for carrying out all other batch experimental studies.

Finally, this study demonstrated the determination of kinetic parameters and correlation coefficient (R^2) values derived from the Lagergren equation, including pseudo-first-order (PFO) and pseudo-second-order (PFO) kinetic model to evaluate the

experimental data. It was found that the adsorption fits well best, either PFO or PSO, according to the R^2 values, which are high enough for both kinetic models ($R^2 > 0.8$). However, R^2 does not guarantee the model acceptability and is not sufficient to determine a suitable kinetic model. Therefore, the evaluation for residues or linear modeling adsorption kinetic errors should be done to avoid the spurious conclusion. Different validation methods were applied to calculate the errors. These validation methods including Sum of Square Error (SSE), Chi-Square (χ^2), Mean Square Error (MSE), Root Means Square Error (RMSE), Normalized Standard Deviation ($\Delta y(\%)$), Average Relative Error (ARE), and Sum of Absolute Error (SAE). Each of these validation methods is a measure of how low the model error is. Consequently, the model would have higher R^2 values and lower values for the other validation methods. Based on this calculation, we could say that La^{3+}, Tb^{3+}, Lu^{3+}, Cu^{2+}, and Zn^{2+} ions adsorbed onto PVPA-10 are better described by PFO rather than PSO kinetic model. This model indicated that one metal ion is exclusively adsorbed onto one unoccupied adsorption site on the PVPA-10 particle surface. We also tried to evaluate the mechanism of metal ions uptake onto PVPA-10 particles. The mechanism of metal ions uptake occurs either by ion exchange or adsorption or by both, depending on the charged state of the adsorbent surface. Last, the adsorption isotherms were investigated by applying Freundlich and Langmuir`s non-linear model. The maximum adsorption of La^{3+}, Tb^{3+}, Lu^{3+}, Cu^{2+}, and Zn^{2+} predicted using Langmuir adsorption isotherm model to be 0.185, 0.097, 0.088, 0.045, and 0.135 mmol g^{-1}, respectively.

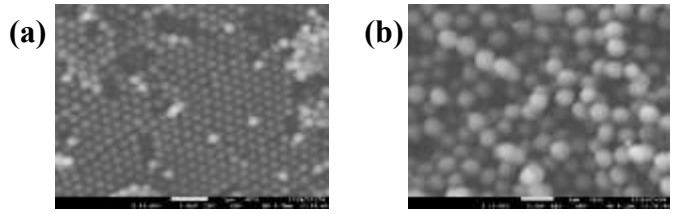

Fig.1. SEM image of the phosphonic acid-functionalized nanoparticle **(a)**, and non-functionalized nanoparticle **(b)**.

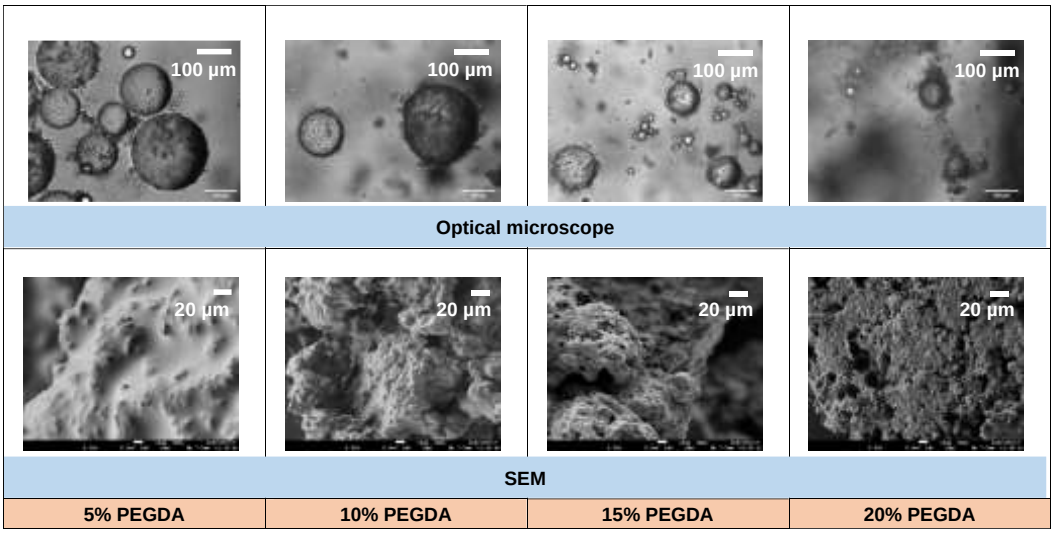

Fig.2. Optical microscope and SEM images of PVPA-PEGDA particles with varying PEGDA content.

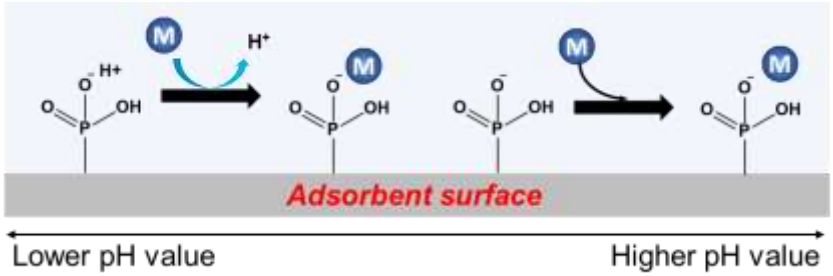

Fig.3. Schematic representation of two different mechanisms of metal ions uptake through ion exchange and adsorption at different pH values.

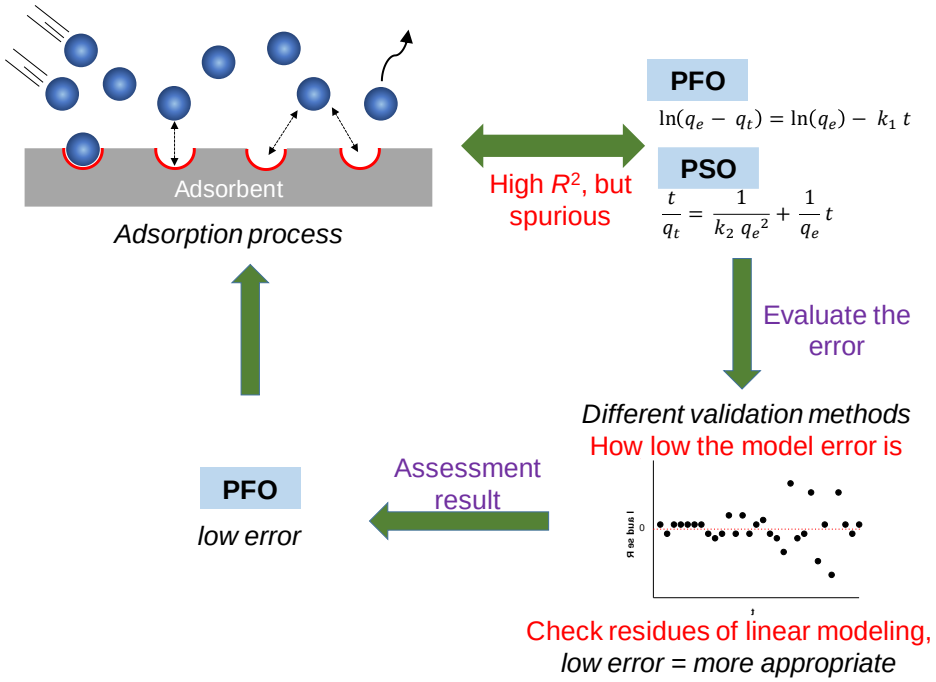

Fig.4. Representation of the framework of thinking to avoid the spurious conclusion in determining the appropriate kinetic model.

Content

Chapter I. General introduction

Polymeric spherical particles have attracted much attention due to their three-dimensional crosslinked polymeric structure, and have been used in numerous applications in several areas [1][2][3]. Their adjustable features and unique behavior make them suitable to produce different types of materials.

Heterogeneous polymerization is a polymerization technique that involves two or more immiscible liquids, in which the starting monomers and resulting polymers form fine dispersion in an immiscible liquid. When two immiscible liquids are mixed, they form an oil-in-water (O/W) or water-in-oil (W/O) system. The heterogeneous polymerization is widely applied for producing a vast amount of polymeric spherical particles. These polymerization techniques, including emulsion, suspension, dispersion, and precipitation polymerization, are usually employed to synthesize such polymer particles. Different polymerization methods produce particles having different size ranges. This study focused solely on emulsion and suspension polymerization methods to prepare the polymeric spherical particles. However, the term of emulsion and suspension is sometimes unclear and confusing for students and non-polymer scientists. Therefore, according to Arshady et al., an arbitrary dividing line between emulsion and suspension is a droplet/ particle size of 1 μm (1000 nm). He explained that the fluids containing droplets/ particles smaller than about 1 μm are known as emulsions, and those containing droplets/ particles larger than about 1 μm are known as suspension [4].

The emulsion polymerization method is initiated by: (1) water-soluble initiator, (2) surfactant, and (3) water as the continuous phase. As a consequence, these combinations are possible to generate an O/W system. Thus, this method is proven to produce

monodisperse polymeric spherical particles with narrow molecular weight distribution. On the other hand, the suspension polymerization method is initiated by: (1) oil-soluble initiator, (2) stabilizer, and (3) oil as the continuous phase. These combinations are possible to produce a W/O system and prepare highly polydisperse polymer particles. Both of these polymerization methods are simple to operate and easy to perform.

Surface-functionalized polymers have attracted widespread interest for many applications [5]. Functionalization of polymer with functional desire groups such as carboxylic acid, sulfonic acid, and phosphonic acid on its surface has dramatically changed the original properties of such polymers. Among numerous functional groups, phosphonic acid groups have found interest in many fields of application because of their attractive physical and chemical properties such as porosity, high surface area, durability, and purity. It is also well known that phosphonic acid-containing polymers could be used as a promising sorbent for metal ions sorption due to their high affinity for many metal ions [6][7][8][9].

Among numerous functional synthetic polymers available, poly(vinylphosphonic acid) (PVPA) and its derivate are growing in interest in many applications. The PVPA indicates challenging properties because of the phosphonic acid functional group`s presence at every repeating unit in its structure. Vinylphosphonic acid (VPA) has a chelate that allows the exchanging of metal ions, and it is possible to apply in heavy metal ions adsorption. Moreover, adsorption has been proven to be a promising treatment process due to its simplicity, high adsorption capacity, selective, low cost, fast, and so on. Adsorption can be used to recover heavy metals even from low-concentration sources.

In Chapter II, phosphonic acid-functionalized on styrene and divinylbenzene were synthesized by the O/W emulsion polymerization method. Fourier transform infrared (FT-

IR) confirmed the structures of the particles, and scanning electron microscopy (SEM) and optical microscope examined the morphology of the particles. Obtaining polymer nanoparticles shows many features such as large specific surface area, high uniformity, spherical with highly monodisperse particles were observed in all systems. The average diameter particle to be 650 ± 30 nm and 310 ± 20 nm for PS-DVB and PS-DVB-VPA, respectively, and polydispersity index (PDI) values are lower than 0.1. The adsorption study was briefly evaluated. As a result, there is no significant difference between the presence and absence of phosphonic acid functional groups on its polymer surface. These findings were probably attributed to there are not having high enough VPA grafted onto PS-DVB nanoparticles.

In Chapter III, crosslinked poly(vinylphosphonic acid) particles were synthesized by the W/O suspension polymerization method using vinyl phosphonic acid (VPA) as monomer and poly(ethylene glycol) diacrylate (PEGDA) as a crosslinking agent. The structure and morphology of the particles were confirmed by FT-IR, SEM, and optical microscope. Furthermore, the adsorption properties, i.e., the kinetic process of the best condition`s sample, and the adsorption isotherms were examined for trivalent (lanthanide series, Ln^{3+} = La^{3+}, Tb^{3+}, and Lu^{3+}) and divalent (Cu^{2+} and Zn^{2+}) metal ions. The adsorption kinetics was best described by either pseudo-first-order (PFO) or pseudo-second-order (PSO) kinetic model according to the correlation coefficient (R^2) values. However, the R^2 value does not guarantee the model acceptability. Therefore, to avoid the spurious conclusion, the residues resulting from a linear fit kinetic model should be evaluated using other validation methods to exhibit how low the model error is. Assessment results for the validation method reveal that the PFO kinetic model is more appropriate to describe the adsorption kinetics of metal ions onto polymer particles. From

the viewpoint of chemical reaction, the PFO kinetic model is more reasonable to explain the reaction mechanism since one metal ion is exclusively adsorbed onto one unoccupied adsorption active site either by ion exchange or adsorption or by both depending on the charged state of the adsorbent surface.

A further aim is to describe equilibrium data using equilibrium isotherm models. The isotherm constants for Freundlich and Langmuir isotherms have been calculated using non-linear equation with the help of Origin software program.

References Chapter I

[1] K. Naseem, Z. Hussain Farooqi, M. Zia Ur Rehman, M. Atiq Ur Rehman, and M. Ghufran, "Microgels as efficient adsorbents for the removal of pollutants from aqueous medium," *Rev. Chem. Eng.*, vol. 35, no. 2, pp. 285–309, 2019, doi: 10.1515/revce-2017-0042.

[2] Z. Dai and T. Ngai, "Microgel particles: The structure-property relationships and their biomedical applications," *J. Polym. Sci. Part A Polym. Chem.*, vol. 51, no. 14, pp. 2995–3003, 2013, doi: 10.1002/pola.26698.

[3] R. A. Meurer *et al.*, "Biofunctional Microgel-Based Fertilizers for Controlled Foliar Delivery of Nutrients to Plants," *Angew. Chemie - Int. Ed.*, vol. 56, no. 26, pp. 7380–7386, 2017, doi: 10.1002/anie.201701620.

[4] R. Arshady, "Suspension, emulsion, and dispersion polymerization: A methodological survey," *Colloid Polym. Sci.*, vol. 270, no. 8, pp. 717–732, 1992, doi: 10.1007/BF00776142.

[5] Z. Zeng, S. Yang, L. Zhang, and D. Hua, "Phosphonate-functionalized polystyrene microspheres with controlled zeta potential for efficient uranium sorption," *RSC Adv.*, vol. 6, no. 78, pp. 74110–74116, 2016, doi: 10.1039/c6ra16219c.

[6] I. Komasawa, T. Otake, and Y. Higaki, "Equilibrium studies of the extraction of divalent metals from nitrate media with di-(2ethylhexyl) phosphoric acid," *J. Inorg. Nucl. Chem.*, vol. 43, no. 12, pp. 3351–3356, 1981, doi: 10.1016/0022-1902(81)80114-5.

[7] M. Matsumoto, K. Yoshizuka, K. Kondo, and F. Nakashio, "Extraction equilibria of copper and zinc with n-8-quinolylsulfonamides," *J. Chem. Eng. Japan*, vol. 17, no. 1, pp. 89–93, 1984, doi: 10.1252/jcej.17.89.

[8] F. Zhang, J. Dai, A. Wang, and W. Wu, “Investigation of the synergistic extraction behavior between cerium (III) and two acidic organophosphorus extractants using FT-IR, NMR and mass spectrometry,” *Inorganica Chim. Acta*, vol. 466, pp. 333–342, 2017, doi: 10.1016/j.ica.2017.06.016.

[9] B. J. Brennan, M. J. Llansola Portolés, P. A. Liddell, T. A. Moore, A. L. Moore, and D. Gust, “Comparison of silatrane, phosphonic acid, and carboxylic acid functional groups for attachment of porphyrin sensitizers to TiO2 in photoelectrochemical cells,” *Phys. Chem. Chem. Phys.*, vol. 15, no. 39, pp. 16605–16614, 2013, doi: 10.1039/c3cp52156g.

Chapter II. Synthesis of phosphonic acid-functionalized nanoparticles by oil-in-water (O/W) emulsion polymerization method

2.1 Introduction

Functionalization of the polymer has attracted much attention due to its potential applications, such as bio-implant [1], sorption [2][3], nanoencapsulation [4][5], sensing [6], the chemical energy stored in fuel cells [7], and others. Functionalization of the polymer with functional desire groups such as carboxylic acid [8][9][10][11], sulfonic acid [12], and phosphonic acid on its surface has dramatically changed the original properties of such polymers. Among numerous functional groups, phosphonic acid groups have found interest in many fields of application because of their attractive physical and chemical properties such as porosity, high surface area, durability, and purity. It is also well known that phosphonic acid-containing polymers could be used as a promising sorbent for metal ions sorption due to their high affinity for many metal ions. However, the ability of homo- or copolymerization of vinyl phosphonate by free radical initiator has been reported to be relatively poor [13].

Many efforts have been made to solve this problem. Several methods have been reported in the preparation of phosphonic acid-containing polymers, including chemical modification [14][15][16][17][18], dispersion polymerization [19][20], and emulsion polymerization [21][22][23].

We notice that the oil-in-water (O/W) emulsion polymerization method has been widely used in various applications to prepare monodisperse polymer particles with narrow molecular weight distribution. This facile method produces smaller particles ranging from 50 nm – 1 μm [24].

In this chapter, phosphonic acid-functionalized on styrene-divinylbenzene copolymer (8 wt% DVB) were synthesized by the O/W emulsion polymerization method. The synthesis and properties of phosphonic acid-functionalized nanoparticles were compared with the particles obtained without phosphonic acid, including adsorption ability for metal ion. The structure and morphology of the functionalized-polymer nanoparticles were confirmed by Fourier transform infrared (FT-IR) spectroscopy and scanning electron microscopy (SEM), and optical microscope. The phosphorous content of the functionalized-polymer nanoparticles was determined by Perkin-Elmer Optima 8300 ICP-Optical Emission Spectrometer.

2.2 Experimental

2.2.1 Materials

Styrene (St) was purchased from Wako Chemical Industries, Ltd (Japan). Divinylbenzene (DVB) was obtained from Sigma-Aldrich Co (New York, USA). Vinylphosphonic acid (VPA, 95%) was purchased from Tokyo Chemical Industry Co., Ltd (Tokyo, Japan). Potassium Persulfate (KPS) and 2,2`azobis (isobutyronitrile) (AIBN) were purchased from Kanto Chemical, Co., Inc (Tokyo, Japan). Hydrochloric acid (HCl) was purchased from Nacalai Tesque, Inc (Kyoto, Japan). Sodium hydroxide (NaOH) was obtained from Fujifilm Wako Pure Chemical Corporation (Osaka, Japan). Ultrapure water was produced by a Direct-Q UV (Millipore, Merck).

2.2.2 Purification of monomer and crosslinking agent

5% NaOH solution was used to purify St and DVB and then followed by washing with water, dried over anhydrous sodium sulfate. All materials were kept in the refrigerator

before being used.

2.2.3 Synthesis of phosphonic acid-functionalized nanoparticles

Phosphonic acid-functionalized nanoparticles, hereafter PS-DVB-VPA, were synthesized by the O/W emulsion polymerization method initiated by KPS: 200 mL three-neck round-bottom flask fitted with a magnetic field stirrer, sample inlet, and nitrogen (N_2) inlet. The flask is charged with 50 mL distilled water (dH_2O), and N_2 is bubbled through dH_2O for 10 min. A mixture of 1 mL St, 88 µL (8 wt% of monomer) DVB, and 6.61 µL (1 wt% of monomer) VPA is added into the flask with magnetic stirring. The mixture was kept under N_2 for 10 minutes to make the emulsion perfectly mixed. Then, the flask is kept under a slightly positive pressure of N_2 to eliminate the inhibiting effect of oxygen before the addition of the initiator. Subsequently, the temperature of the reaction mixture remains steady at 70^{o}C, and then 9.09 mg (1 wt% of monomer) KPS dissolved in 5 mL dH_2O is added. The mixture is stirred continuously at 100 rpm and becomes a milky colloidal solution, namely PS-DVB-VPA. Polymerization was completed in approximately ten hours. The same procedure accomplished preparing the PS-DVB nanoparticles without involving the VPA as a functional agent, and the reactions recipe is presented in **Table 1**.

In order to remove the buffer salt, a by-product from the initiator, and low Mw of water-soluble reactant, the as-prepared particles are dialyzed against dH_2O for three days using a dialysis bag (Mw cut off = 12,000 – 14,000 g mol^{-1}).

2.2.4 Characterization of phosphonic acid-functionalized nanoparticles

An optical microscope and SEM were used to observe the surface morphology, and the size and polydispersity were analyzed using the ImageJ program. FT-IR was used to

identify the chemical bond of the polymer nanoparticles. Perkin-Elmer Optima 8300 ICP-Optical Emission Spectrometer was used to determine the phosphorous content of the phosphonic acid-functionalized nanoparticles.

2.3 Result and discussion

2.3.1 Synthesis of phosphonic acid-functionalized nanoparticles

The polymerization reaction of phosphonic acid-functionalized nanoparticles from St and DVB under nitrogen gas using KPS as an initiator was carried out. The polymer formed at the end of the reaction appeared milky white colloidal solution. The time of polymerization was terminated after ten hours.

Table 1. Recipes of synthetic polymer particles.

Sample No	Styrene (mL)	DVB (mol)	VPA (mol)	Namely
I	1	6.14×10^{-4}	-	PS-DVB
II	1	6.14×10^{-4}	8.50×10^{-5}	PS-DVB-VPA

2.3.2 Characterization

2.3.2.1 Fourier Transform-Infra Red (FT-IR) spectra

The characteristic absorption band of St and DVB were observed in the FT-IR spectra of PS-DVB nanoparticles. FT-IR spectra show a peak at 3029 cm^{-1} is attributed to aromatic C-H stretching, and a peak around 2936 cm^{-1} might be due to aliphatic C-H stretching. A sharp peak with significant intensity appeared at 1603 cm^{-1}, which indicates C=C stretching of the styrene ring. Multi-peak around 1492 – 1452 cm^{-1} is ascribed to the aromatic C-H stretching due to the presence of a phenyl ring. The narrow peak with high intensity at 780 – 700 cm^{-1} is due to the phenyl ring`s aromatic substitution. Stretching

absorptions usually produce more substantial peaks than bending; however, the weaker bending absorptions can help differentiate similar types of bonds (e.g., aromatic substitution). The presence of aromatic C-H, aliphatic C-H, and C=C peaks in FT-IR spectra of PS-DVB nanoparticles conforms with the reported literature. These results confirm that the PS-DVB was successfully synthesized by the O/W emulsion polymerization method.

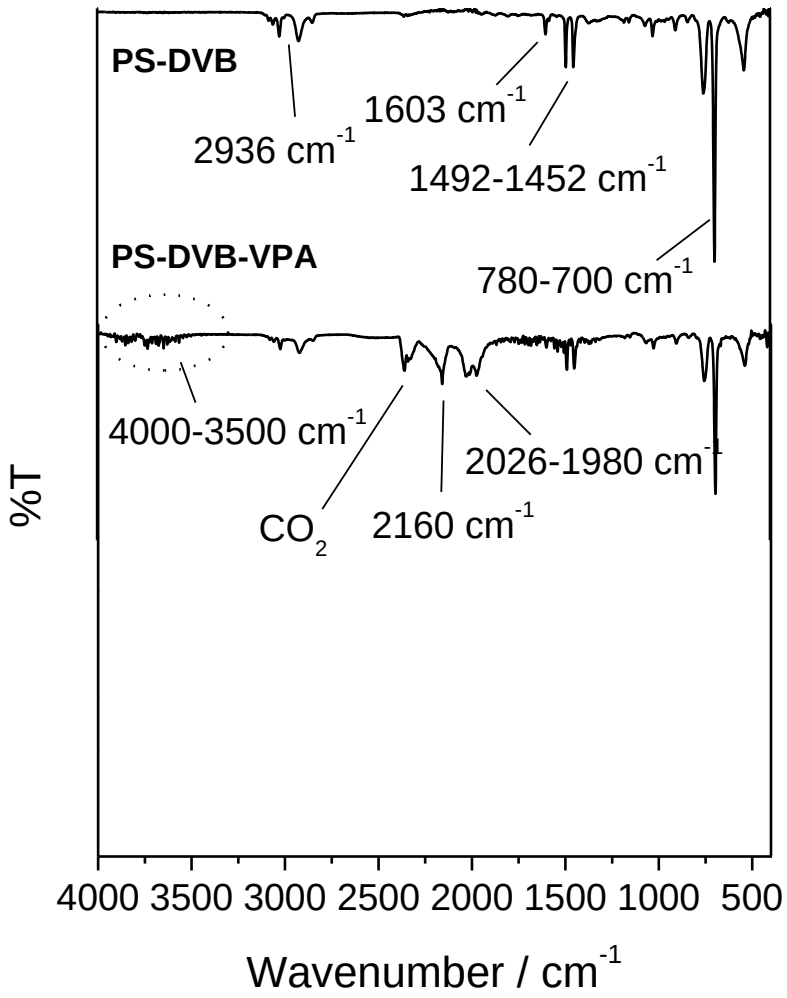

Figure 2.1. FT-IR spectra of the PS-DVB and PS-DVB-VPA nanoparticles.

The main distinction of PS-DVB-VPA compared to that of PS-DVB is the exclusive presence of sharp peaks and intense bands between the region 4000 – 3500 cm^{-1} due to

the vibration of –OH from phosphonic acid functional groups. Other possibilities are that the intramolecular –OH bond will appear sharp peak around this region. In addition to this, in most cases, the –OH peak`s characteristic is a broad peak appearing above 3000 cm^{-1}. However, obtaining spectrum is different from most of containing –OH spectrum. The larger compounds could explain this condition that may sterically hinder hydrogen bonding, preventing exchange. In these situations, the broad –OH peak is replaced by a sharp spectrum around 4000 – 3500 cm^{-1}. To be agreed with this statement, **Figure 2.1** shows a sharp peak spectrum in the range between 4000 – 3500 cm^{-1}.

The multi-peak band between 2160 – 1980 cm^{-1} can be assigned to be P-OH stretching and hydrogen bonding of P-OH surface among of phosphonic acid functional group on the polymer surface. The FT-IR result reveals that PS-DVB-VPA was successfully synthesized through the O/W emulsion polymerization method.

2.3.2.2 Elemental analysis

The phosphorous content of the phosphonic acid-functionalized nanoparticles (PS-DVB-VPA) was obtained by oxidative decomposition with mixed acid under elevated temperature. The phosphorous content was used to determine their functionalization degree. In this study, the phosphorous content in the PS-DVB-VPA to be less than 0.5 wt% P, which indicates that the phosphonate content is less than the detection limit. This result is not a denial of the presence of surface phosphonate groups on the polymer surface, as inferred from the FT-IR result.

2.3.2.3 Particle morphology

An optical microscope type Olympus IX51 inverted microscope was used to observe the

polymer particles. Due to the polymer solution being too concentrated, the colloidal solution was diluted in water. As a result, the microscope instrument quickly observes the particles, as inferred in **Figure 2.2**.

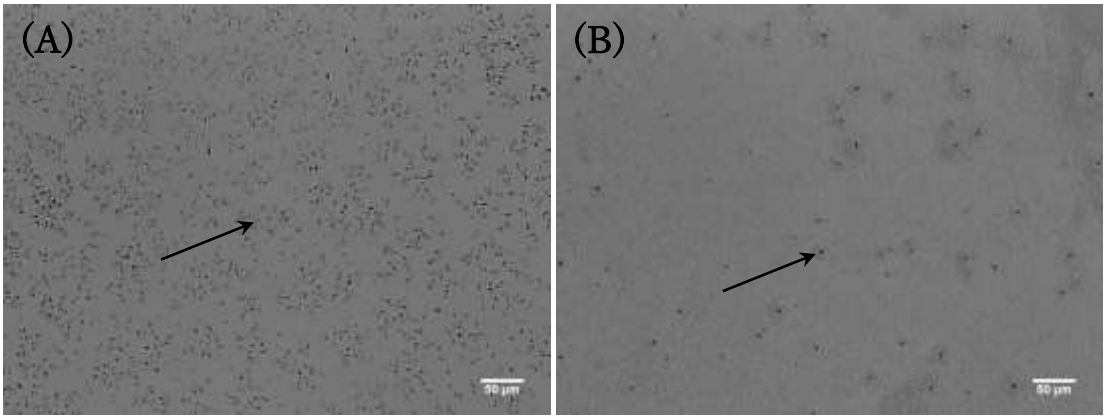

Figure 2.2. Optical microscope images of (A). PS-DVB; and (B). PS-DVB-VPA nanoparticles (An arrow denotes a particle).

SEM analyzed the morphology and particle size, as shown in **Figure 2.3**. ImageJ software was used to investigate the area and particle distribution. Then, the diameter distribution was calculated using Origin software. Finally, average nanoparticles size, standard deviation (σ), and polydispersity index (PDI) values were obtained by computational analysis, as summarized in **Table 2**.

Table 2. The overall calculation for diameter distribution using Origin software and other parameter values for PS-DVB and PS-DVB-VPA nanoparticles.

Diameter distribution by using Origin	**Computational Analysis**
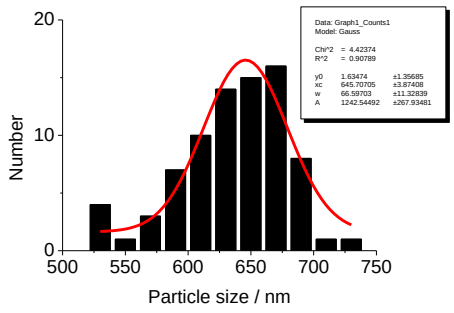	■ PS-DVB Average NP size (X_c) = **645.71 nm** W = 66.60 nm Standard Deviation (σ) = W/2 = 33.30 Therefore, Average NP size with error = $X_c \pm \sigma$ = 645.71 ± 33.30 nm Polydispersity = (σ/X_c) x 100% = (33.30/645.71) x 100% = 5.16 %

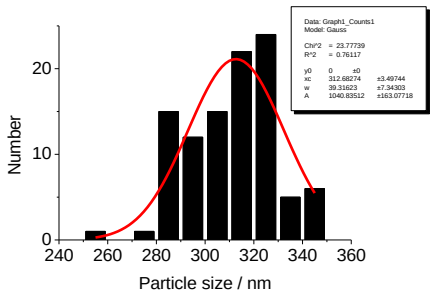

■ PS-DVB-VPA

Average NP size (X_c) = **312.68 nm**

W = 39.32 nm

Standard Deviation (σ) = W/2 = 19.66

Therefore, Average NP size with error = $X_c \pm \sigma$ = 312.68 ± 19.66 nm

Polydispersity = (σ/X_c) x 100% = (19.66/312.68) x 100% = 6.29 %

The morphology of PS-DVB and PS-DVB-VPA nanoparticles was investigated using SEM. Obtaining polymer nanoparticles shows many features such as large specific surface area, high uniformity, and spherical with highly monodisperse particles. All systems observed particle sizes with an average diameter of 650 ± 30 nm and 310 ± 20 nm for PS-DVB and PS-DVB-VPA, respectively. The values of the polydispersity index (PDI) are lower than 0.1 for all obtaining polymer particles. This result indicates that the size is monodisperse for the polymer nanoparticles. The functional agents affected the polymer characteristic. In the case of VPA as a functional agent, very few particles in the order 300 nm were observed. The particle size decreased when VPA was employed as the functional agent during synthesis. Besides functional agents. The VPA can also act as emulsifier agents that assistance the formation of micelle in solution. In the emulsion polymerization mechanism, the reaction occurs mainly inside the micelle. When emulsifier concentration increases, more micelles are formed, and the number of polymer particles per unit volume increases, and thus, the polymerization rate increases. Shortly, using too much emulsifier may inhibit the growth of polymer particles [25].

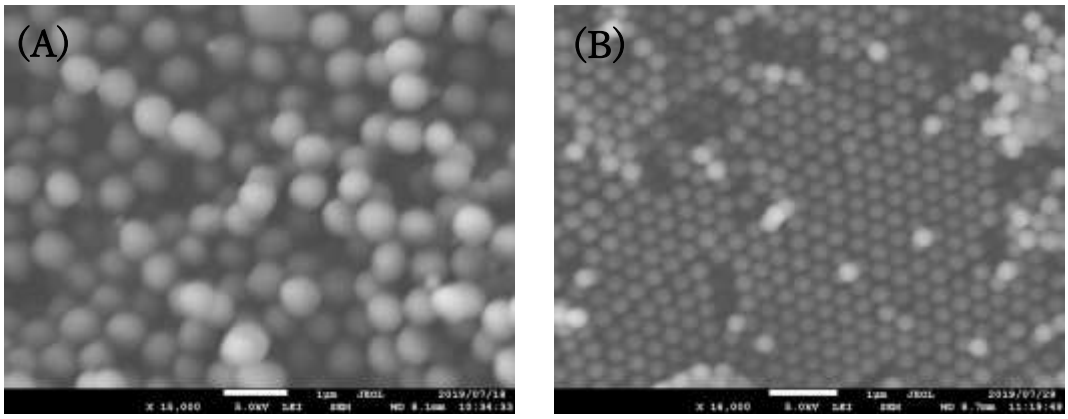

Figure 2.3. SEM images of (A). PS-DVB; and (B). PS-DVB-VPA nanoparticles.

2.3.3 Adsorption study

pH is an important factor affecting the adsorption of cations from aqueous solutions. Obtained polymeric particles were tested the adsorption ability based on the precipitate formed.

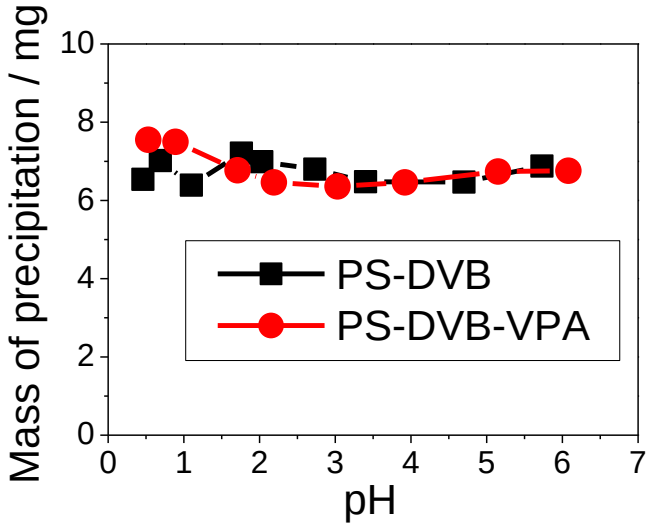

Figure 2.4. The effect of pH on the precipitated polymer with presence and absence of phosphonic acid functional groups on the polymer surface (Experimental condition: Tb^{3+} concentration 1 x 10^{-3} mol L^{-1}; volume Tb^{3+} 0.5 mL; volume polymer used 0.5 mL).

As a result, there is no significant difference between the presence and absence of

phosphonic acid functional groups on the polymer surface. These findings were probably attributed to there are not having high enough VPA grafted onto PS-DVB nanoparticles, which is in line with the elemental analysis result that reveals low content of phosphorous in the PS-DVB-VPA.

2.4 Summary

We successfully synthesized phosphonic acid-functionalized nanoparticles using the oil-in-water (O/W) emulsion polymerization method. FT-IR confirmed the structures of the particles, and SEM and optical microscope examined the morphology of the particles. Obtained polymer nanoparticles show many features such as large specific surface area, high uniformity, and spherical with highly monodisperse particles. The particle size was observed in all systems with an average diameter of 650 ± 30 and 310 ± 20 nm for PS-DVB and PS-DVB-VPA, respectively. Then, polydispersity index (PDI) values that are lower than 0.1 indicate the uniformity of the particles.

It shows that obtained polymer nanoparticles prepared by the O/W emulsion polymerization method have the poor ability in adsorption ability. The effect of the presence and absence of phosphonic acid functional groups on the polymer surface is unclear according to precipitated polymers.

2.5 References Chapter II

[1] A. Zeller *et al.*, "Nanostructured coatings by adhesion of phosphonated polystyrene particles onto titanium surface for implant material applications," *ACS Appl. Mater. Interfaces*, vol. 2, no. 8, pp. 2421–2428, 2010, doi: 10.1021/am1004305.

[2] A. Popa, C. M. Davidescu, P. Negrea, G. Ilia, A. Katsaros, and K. D. Demadis, "Synthesis and characterization of phosphonate ester/phosphonic acid grafted styrene - Divinylbenzene copolymer microbeads and their utility in adsorption of divalent metal ions in aqueous solutions," *Ind. Eng. Chem. Res.*, vol. 47, no. 6, pp. 2010–2017, 2008, doi: 10.1021/ie070886g.

[3] J. Florek, S. Giret, E. Juère, D. Larivière, and F. Kleitz, "Functionalization of mesoporous materials for lanthanide and actinide extraction," *Dalt. Trans.*, vol. 45, no. 38, pp. 14832–14854, 2016, doi: 10.1039/c6dt00474a.

[4] Y. Luo and X. Zhou, "Nanoencapsulation of a hydrophobic compound by a miniemulsion polymerization process," *J. Polym. Sci. Part A Polym. Chem.*, vol. 42, no. 9, pp. 2145–2154, 2004, doi: 10.1002/pola.20065.

[5] N. Bechthold, F. Tiarks, M. Willert, K. Landfester, and M. Antonietti, "Miniemulsion polymerization: Applications and new materials," *Macromol. Symp.*, vol. 151, pp. 549–555, 2000, doi: 10.1002/1521-3900(200002)151:1<549::AID-MASY549>3.0.CO;2-D.

[6] X. Yang, L. W. Zhu, L. S. Wan, J. Zhang, and Z. K. Xu, "Surface functionalization of cross-linked polystyrene microspheres via thiol-ene 'click' reaction and assembly in honeycomb films for lectin recognition," *J. Mater. Res.*, vol. 28, no. 4, pp. 642–650, 2013, doi: 10.1557/jmr.2012.420.

[7] Z. Yang, H. Peng, W. Wang, and T. Liu, “Crystallization behavior of poly(ε-caprolactone)/layered double hydroxide nanocomposites,” *J. Appl. Polym. Sci.*, vol. 116, no. 5, pp. 2658–2667, 2010, doi: 10.1002/app.

[8] G. Liu and P. Liu, “Preparation of carboxyl-coated polystyrene nanoparticles using oleic acid,” *IET Nanobiotechnology*, vol. 3, no. 2, pp. 23–27, 2009, doi: 10.1049/iet-nbt.2008.0009.

[9] N. M. Sekerak *et al.*, “Size control of cross-linked carboxy-functionalized polystyrene particles: Four orders of magnitude of dimensional versatility,” *Eur. Polym. J.*, vol. 101, no. January, pp. 202–210, 2018, doi: 10.1016/j.eurpolymj.2018.01.028.

[10] C. Dire, S. Magnet, L. Couvreur, and B. Charleux, “Nitroxide-mediated controlled/living free-radical surfactant-free emulsion polymerization of methyl methacrylate using a poly(methacrylie acid)-based macroalkoxyamine initiator,” *Macromolecules*, vol. 42, no. 1, pp. 95–103, 2009, doi: 10.1021/ma802083g.

[11] S. Zhu, U. Panne, and K. Rurack, “A rapid method for the assessment of the surface group density of carboxylic acid-functionalized polystyrene microparticles,” *Analyst*, vol. 138, no. 10, pp. 2924–2930, 2013, doi: 10.1039/c3an36578f.

[12] X. Zhang *et al.*, “Polystyrene sulphonic acid resins with enhanced acid strength via macromolecular self-assembly within confined nanospace,” *Nat. Commun.*, vol. 5, pp. 1–9, 2014, doi: 10.1038/ncomms4170.

[13] R. M. Pike and R. A. Cohen, “Organophosphorus Polymers . I . Peroxide-Initiated Vinylphosphonate *,” vol. X, pp. 531–538, 1960.

[14] A. Głowinska and A. W. Trochimczuk, “Polymer-supported phosphoric, phosphonic and phosphinic acids—from synthesis to properties and applications

in separation processes," *Molecules*, vol. 25, no. 18, 2020, doi: 10.3390/molecules25184236.

[15] B. T. Benkhaled, T. Montheil, V. Lapinte, and S. Monge, "Hydrosoluble phosphonic acid functionalized poly(2-ethyl-2-oxazoline) chelating polymers for the sorption of metallic cations," *J. Polym. Sci.*, vol. 58, no. 20, pp. 2875–2886, 2020, doi: 10.1002/pol.20200487.

[16] A. W. Trochimczuk, "Synthesis of functionalized phenylphosphinic acid resins through Michael reaction: Part II. Resins with multidentate ligands," *React. Funct. Polym.*, vol. 48, no. 1–3, pp. 141–148, 2001, doi: 10.1016/S1381-5148(01)00049-9.

[17] X. Liu, J. Li, X. Wang, C. Chen, and X. Wang, "High performance of phosphate-functionalized graphene oxide for the selective adsorption of U(VI) from acidic solution," *J. Nucl. Mater.*, vol. 466, pp. 56–64, 2015, doi: 10.1016/j.jnucmat.2015.07.027.

[18] C. M. Davidescu *et al.*, "Behaviour of Polymeric Resins Bearing Various Phosphorus Containing Ligands towards Metal Ions from Aqueous Solutions," vol. 55, no. 69, pp. 32–36, 2010.

[19] A. Hanisch, P. Yang, A. N. Kulak, L. A. Fielding, F. C. Meldrum, and S. P. Armes, "Phosphonic Acid-Functionalized Diblock Copolymer Nano-Objects via Polymerization-Induced Self-Assembly: Synthesis, Characterization, and Occlusion into Calcite Crystals," *Macromolecules*, vol. 49, no. 1, pp. 192–204, 2016, doi: 10.1021/acs.macromol.5b02212.

[20] J.-S. Song, L. Chagal, and M. A. Winnik, "Monodisperse micrometer-size carboxyl-functionalized polystyrene particles obtained by two-stage dispersion

polymerization," *Macromolecules*, vol. 39, no. 17, pp. 5729–5737, 2006, doi: 10.1021/ma052550f.

[21] L. Breucker, K. Landfester, and A. Taden, "Phosphonic Acid-Functionalized Polyurethane Dispersions with Improved Adhesion Properties," *ACS Appl. Mater. Interfaces*, vol. 7, no. 44, pp. 24641–24648, 2015, doi: 10.1021/acsami.5b06903.

[22] D. Hua, J. Tang, J. Jiangs, X. Zhu, and R. Bai, "A facile approach for preparation of phenylphosphinic acid-functionalized pst microspheres by emulsion polymerization using amphiphilic macro-RAFT agent as emulsifier," *Macromolecules*, vol. 42, no. 22, pp. 8697–8701, 2009, doi: 10.1021/ma9018334.

[23] A. Ziegler, K. Landfester, and A. Musyanovych, "Synthesis of phosphonate-functionalized polystyrene and poly(methyl methacrylate) particles and their kinetic behavior in miniemulsion polymerization," *Colloid Polym. Sci.*, vol. 287, no. 11, pp. 1261–1271, 2009, doi: 10.1007/s00396-009-2087-z.

[24] R. Arshady, "Suspension, emulsion, and dispersion polymerization: A methodological survey," *Colloid Polym. Sci.*, vol. 270, no. 8, pp. 717–732, 1992, doi: 10.1007/BF00776142.

[25] C. Zhao, H. Okada, and R. Sugimoto, "Polymerization of styrene in aqueous system using a diethylzinc and 1,10-phenanthroline complex," *Polymer (Guildf).*, vol. 154, no. August, pp. 211–217, 2018, doi: 10.1016/j.polymer.2018.09.019.

2.6 List of figure

2.7 List of table

Chapter III. Synthesis of crosslinked poly(vinylphosphonic acid) particles by water-in-oil (W/O) suspension polymerization method and their adsorption properties of metal ions

3.1 Introduction

Polymeric particles could be used as a low-cost potential adsorbent and have attracted much attention due to their widespread applications in personal care products [1], bone tissue scaffolds [2], coatings technology [3], drug delivery [4], agriculture as delivery of nutrient to plants [5], and chemical separation process [6][7][8]. Polymer particles based on a polymeric network carrying ionic groups such as carboxylic acid, sulfonic acid, and phosphonic acid moieties are referred to as more promising materials. Therefore, considerable effort has been devoted to developing new polymeric materials, such as functional synthetic polymers. Among many functional synthetic polymers known today, poly(vinyl phosphonic acid) (hereafter: PVPA) and its derivate are growing in interest for various applications.

Although PVPA may be considered one of the simplest polymer diprotic acids and has solely represented phosphorous-containing polymer particles in the commercial market so far, only a limited number of reports on the potential use are available in the form of particles [9][10].

The PVPA indicates challenging properties because of the phosphonic acid functional group's presence at every repeating unit in its structure. The PVPA-based products have been used in many applications such as medicine, scale inhibition, and separation. However, the existing literature indicates that few studies have been performed on phosphonic acid-based microgel sorption capabilities. Kaltbeitzel et al. has been reported

the synthesis of PVPA by free-radical polymerization and tested their performance on water sorption. Their water sorption capacities are ~15 wt%, which means 0.8 water molecules per phosphonic acid group [11]. Najafi et al. designed PVPA microgel crosslinked with PEGMEMA and used them for ethanol and methanol adsorption up to 15.1 and 17.8 g g^{-1}, respectively [12]. Kwak et al. investigated the isotherm, kinetic, and thermodynamic parameters of indium adsorption by poly(vinyl phosphonic acid-co-acrylic acid) microgels crosslinked with *N*-*N*`-methylene-bisacrylamide (MBAA), which resulted in 0.78 mmol g^{-1} resin of adsorption capacity at optimum condition [13]. They also reported 0.70 mmol g^{-1} resin of indium adsorption capacity for the poly(vinyl phosphonic acid-co-methacrylic acid) microgels crosslinked with poly(ethylene glycol) diacrylate (PEGDA) as a crosslinker that they developed [14]. Sahiner et al. investigated the short and high amounts of uranyl uptake using PVPA microgels [15]. Anil et al. reported special dyes sorption capacity of crosslinked-PVPA that they designed by varying crosslinker fractions [16].

Rare earth elements (REEs) include the periodic table lanthanide series, have been widely used in various applications. As a result of their usage, more and more REEs are getting into the environment, food chain, and organisms. The concentration of REEs in environmental samples such as soil, atmosphere, and body water increases over time through anthropogenic agents and unregulated human interference.

A number of physicochemical treatment have been used for REEs removal, such as extraction [17], ultrafiltration [18], ion-exchange [19], and adsorption [20][21]. Among the available methods, adsorption has been proven to be a promising treatment process due to its simplicity, high adsorption capacity, selective, low cost, fast, and more of the same. Adsorption can be used to recover the REEs even from low-concentration sources.

However, adsorption of trivalent metal ions, on the other hand, had not been studied as extensively as that of divalent metal ions. Specifically, there are no reports yet for lanthanide ion sorption activity for PVPA-based microgels so far to the best of our knowledge.

Water-in-oil (W/O) suspension polymerization method is one part of the heterogeneous polymerization technique that allowed to produce a vast amount of polymeric particles with a range of 10 μm – 5 mm [22][23], simple to operate and easy to perform. However, its application is limited due to the large particle size, size distribution, and high polydispersity index (PDI) value. Higher the value of PDI, the higher the level of dispersion in particle size, which is usually not required. Numerous reports on the preparation of these materials have published in the literature. Kesenchi et al. reported the synthesis of poly[(ethylene glycol dimethacrylate)-co-acrylamide] by suspension polymerization [24], and Tuncel et al. described the preparation of poly(ethylene glycol) methacrylate with the same method [25].

In this chapter, the particles were synthesized by the water-in-oil (W/O) suspension polymerization method using vinyl phosphonic acid (VPA) as monomer and poly(ethylene glycol) diacrylate (PEGDA) as a crosslinking agent. VPA has a chelate that allows the exchanging of metal ions, and it is possible to synthesize by radical polymerization due to its vinyl group. Furthermore, the adsorption properties, i.e., the kinetic process of the sample's best conditions, were examined for trivalent (lanthanide series, Ln^{3+} = La^{3+}, Tb^{3+}, and Lu^{3+}) and divalent (Cu^{2+} and Zn^{2+}) metal ions. An analysis of the kinetic data is essential because the kinetics describe the uptake of the rate of the adsorbate. The effect of parameters, such as crosslinker content, initial solution pH, contact time, and initial metal concentration, was studied to estimate the kinetic

parameters. The structure and morphology of the particles were confirmed by Fourier transform infrared (FT-IR) spectroscopy, scanning electron microscopy (SEM), and optical microscope. The phosphorous content of the functionalized-polymer nanoparticles was determined by Perkin-Elmer Optima 8300 ICP-Optical Emission Spectrometer.

3.2 Experimental

3.2.1 Materials

Vinylphosphonic acid (VPA, 95%) and benzoyl peroxide (BPO, 75%) were purchased from Tokyo Chemical Industry Co., Ltd (Tokyo, Japan). Poly(ethylene glycol) diacrylate (PEGDA, number average molecular weight (M_n) 250) and poly(vinyl alcohol) (PVA, M_n 89000 – 98000, 99% hydrolyzed) were obtained from Sigma-Aldrich Co (New York, USA). Silicone oil (KF-96-3000 CS, KF-96-1000 CS, KF-96-100 CS) was purchased from Shin-Etsu Chemical Co., Ltd (Tokyo, Japan). Colorimetric complexing reagents, 2,7-Bis(4-chloro-2-phosphonophenyl-azo)-1,8-dihydroxy-3,6-napthalene-disulfonic acid, (Chlorophosphonazo-III, CPA-III) and 2-(5-Bromo-2-pyridylazo)-5(N-propyl-N-sulfopropylamino)phenol, disodium salt (5-Br-PAPS) were purchased from Dojindo Laboratories (Kumamoto, Japan). $LaCl_3.7H_20$ (99,9%), $TbCl_3.6H_2O$ (99.9%), $LuCl_3.6H_2O$ (99,99%), $CuCl_2$, and $ZnSO_4.7H_2O$, toluene and NaOH were obtained from Fujifilm Wako Pure Chemical Corporation (Osaka, Japan). K_2HPO_4, KH_2PO_4, and hydrochloric acid were purchased from Nacalai Tesque, Inc (Kyoto, Japan). Ultrapure water was produced by a Direct-Q UV (Millipore, Merck).

3.2.2 Synthesis of crosslinked poly(vinylphosphonic acid) particles

The crosslinked PVPA with PEGDA was synthesized by water-in-oil (W/O) suspension polymerization via free-radical polymerization of VPA in the presence of PEGDA as a crosslinker and BPO an initiator. Several molar fractions of PEGDA, from 5% to 20% molar ratio concerning VPA, were used to reveal the effect of PEGDA on the flexibility, functionalities, and metal sorption activity of the crosslinked particle. The amount of all reagents is represented in **Table 3**. The polymerization was conducted in a 500 mL three-neck round-flask equipped with a mechanical stirrer, a condenser, a nitrogen inlet, and a thermometer. All the reagents were used without further purification. Two types of different solutions were prepared. Firstly, the aqueous droplet was prepared by: VPA and PEGDA were dissolved into a mixture of 4 mL distilled water and PVA at 65ºC for 30 min. Secondly, BPO was dissolved in 2 mL of toluene and then put into 20 mL of silicone oil, which acts as a continuous phase. This continuous phase mixture was placed under vigorous agitation and backfilled with nitrogen gas for 10 minutes to keep the inner condition. Finally, the aqueous droplet was added into the continuous phase, which allows the water-in-oil (W/O) formation while nitrogen keeps flowing before polymerization. The polymerization was performed with airtight equipment at 65ºC for three hours.

The particle was washed three times with toluene to remove silicone oil and BPO on the particle surface. Then, it is continued by washing using methanol three times to remove unreacted monomers and crosslinker. Each of the step, the solution was centrifuged at 4000 rpm for 10 min to separate the phase. All the particles were dried under a vacuum at least 18 hours.

The synthetic yield of the obtaining particle was determined by the equation as follows:

$$\textbf{Synthetic yield } (\%) = \frac{\boldsymbol{W_d}}{\boldsymbol{W_m}} \boldsymbol{x\ 100} \qquad \text{Equation 1}$$

Where W_d is the weight of the clean and dry polymer (g), and W_m is the initial weight of the monomer (g).

3.2.3 Batch adsorption studies

In the metal ions adsorption study, i.e., La^{3+}, Tb^{3+}, Lu^{3+}, Cu^{2+}, and Zn^{2+}, batch adsorption experiments were performed in a set of amber glass Erlenmeyer flasks filled with metal ion solution (10 mL) and placed on an orbital shaker (300 rpm) at room temperature. Samples were immersed into the flask, and the adsorption process was allowed to take place with a specified time. The initial pH solution was adjusted using 1M of HCl or 1M of NaOH solution. At pre-determined time intervals, aliquots were taken out, and their absorbencies were measured to determine the remaining metal ions in the solution.

3.2.3.1 Procedure for determination of trivalent metals (La^{3+}, Tb^{3+}, and Lu^{3+}) in aqueous solution

1 mL aliquots were taken out and complexed with CPA-III. The pH was adjusted to acidic conditions (approximately 1.2 ~ 1.5) using 1M of HCl and total volume precisely 10 mL with the addition of water. The measurement of the absorbance was therefore carried out in 10 min after the addition of CPA-III.

The spectrophotometer was calibrated for each set of experiments using six CPA-III-metal complex solutions with metal ion's final concentrations ranging from 0 – 1 x 10^{-5} mol L^{-1}. Meanwhile, CPA-III final concentration was kept constant, 5 x 10^{-5} mol L^{-1}.

3.2.3.2 Procedure for determination of divalent metals (Cu^{2+} and Zn^{2+}) in aqueous

solution

1 mL aliquots were taken out and complexed with 1 mL of 5-Br-PAPS solution and 1mL buffer phosphate pH 8, and then total volume precisely 10 mL with the addition of water. The measurement of the absorbance was therefore carried out in 10 min after the addition of 5-Br-PAPS.

The spectrophotometer was calibrated for each set of experiments using five 5-Br-PAPS-metal complex solutions with metal ion final concentrations ranging from 0 – 1 x 10^{-5} mol $L^{-1,}$ and 5-Br-PAPS final concentration was kept constant of 4 x 10^{-5} mol L^{-1}.

The amount of metal ions adsorbed per gram of adsorbent at equilibrium, q_e in mmol g^{-1}, was evaluated using according to the following equation:

$$\boldsymbol{q_e(mmol\ g^{-1}) = \frac{(C_0 - C_e)\ V}{m}} \qquad \text{Equation 2}$$

Where C_0 is the initial metal ion concentration and C_e is equilibrium metal ion concentration at specific contact time in solution; V is the volume of metal ion solution (L); m is mass of PVPA-10 particle in the solution (g).

The amount of metal ions adsorbed at several intervals in contact time, and the percent extraction (%E_A) were calculated using the following equations:

$$\boldsymbol{q_t(mmol\ g^{-1}) = \frac{(C_0 - C_t)\ V}{m}} \qquad \text{Equation 3}$$

$$\boldsymbol{\%E_A = \frac{C_0 - C_t}{C_0}\ x\ 100} \qquad \text{Equation 4}$$

Where C_t is metal ion concentration in solution at different period *t*.

The effect of PEGDA content (5, 10, 15, and 20% molar ratio concerning VPA),

initial pH solution (1 – 6), contact time (0 – 720 min), initial metal concentration (5 x 10^{-5} – 1 x 10^{-3} mol L^{-1}), and the amount of adsorbent was kept constant at 20 mg on the adsorption process were investigated to get the optimum condition. All the experiments were performed in triplicate (n = 3).

Table 3. Synthesis conditions of crosslinked poly(vinylphosponic acid) particles.

Sample code	Monomer	Crosslinking	Stabilizer	Initiator
	VPA	PEGDA	PVA	BPO
PVPA-5	12.68 mmol	5 % molar ratio of VPA	0.01 % molar ratio of VPA	1 % molar ratio of VPA
PVPA-10		10 % molar ratio of VPA		
PVPA-15		15 % molar ratio of VPA		
PVPA-20		20 % molar ratio of VPA		

3.3 Result and discussion

3.3.1 Synthesis of crosslinked poly(vinylphosphonic acid) particles

VPA is a hydrophilic monomer possessing two pK_a values (2.74 and 7.34), and protic solvents may be considered suitable solvents, such as water and alcohols. However, VPA cannot be polymerized in water or methanol as the presence of water is reported to negatively affect the polymerization of VPA[9][26]. Crosslinked poly(vinylphosphonic acid) particles were successfully prepared in W/O suspension polymerization. In this process, an aqueous solution of the monomer(s) is emulsified under agitation in a continuous oil phase. Steric stabilizers are employed, and the polymerization is initiated using, in general, oil-soluble initiators at a temperature of 65ºC for three hours. To the best of our knowledge, the presence of stabilizers hinders the coalescence of monomer droplets and the adhesion of partially polymerized particles during the course of

polymerization, so that the solid bead may be produced in the same way spherical form in which the monomer was dispersed in the aqueous phase.

In this study, W/O suspension polymerization was carried out using silicone oil as a continuous phase, which provided a suitable viscosity to prevent aggregation. Viscous silicone oil was used to facilitate polymerization reaction. The addition of viscosity can result in an increase in droplet stability by decreasing the droplet collision frequency.

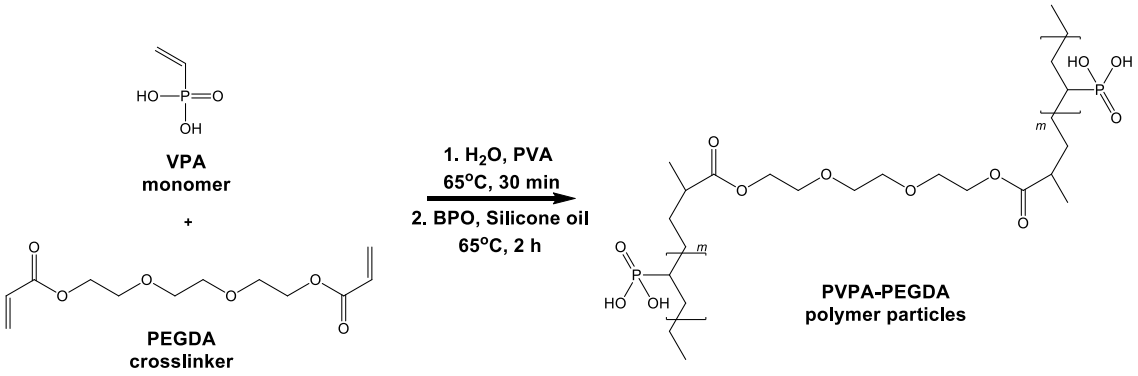

Figure 3.1. Schematic illustration for the synthesis of poly(vinylphosphonic acid)-poly(ethylene glycol) diacrylate polymer particles.

3.3.1.1 Selection of organic solvent

The key to the success of this method is to select a suitable continuous phase. A continuous phase with a high viscosity is required in order to avoid the coalescence of dispersed droplets. The kinematic viscosity of silicone oil used in this experiment is 100 $mm^2\ s^{-1}$, much higher than conventional liquid media, such as water and toluene. So the silicone oil can resist the movement of the droplets, and particles without agglomeration are obtained. Moreover, the significant difference in viscosity between pre-polymerization droplets (approximately 0.89 mPa s) and silicone oil (96.5 mPa s) is suggested a vigorous stirring process to produce a homogeneous emulsion.

On the other hand, the density of pre-polymerization droplets (0.90 g cm^{-3}) is slightly

lower than silicone oil (0.97 g cm^{-3}), so the droplets rise slowly in silicone oil. During the polymerization, the density of the droplets increases gradually, and the movement of droplets slows. After the density of the polymerized droplets becomes higher than that of silicone oil, they begin to sink. Other reasons silicone oil is suitable for dispersing phase are its non-polarity, insolubility with the pre-polymerization mixture, and low cost [27].

Initially, spherical water droplets are formed in the Water-in-Oil (W/O) system. The radius of the droplet is a. A stirring of the dispersion medium causes the droplet shape change from sphere to ellipsoid, where L and B are the length of the major axis and minor of the ellipsoid, respectively. Taylor proposed the following equation to express the shape of the droplet [28]:

$$\frac{L-B}{L+B} = \frac{Ga\eta}{2\gamma}\frac{19\eta_i + 16\eta}{16\eta_i + 16\eta} \qquad \text{Equation 5}$$

Where G is the shear rate, η and η_i are the viscosities of the dispersion medium (oil phase) and the dispersed phase (water phase), respectively, and γ is the interfacial tension. Taylor mentioned that the difference between L and B would distort the particle shape. At the higher ratio (L – B) / (L + B), the droplet become bursting and decompose into stable small droplets.

We also successfully prepared crosslinked poly(vinylphosphonic acid) particles by silicone oils with high viscosity (970 and 2910 mPa s for KF-96-1000CS and KF-96-3000CS, respectively) as the continuous phase. However, the difficulty of removing silicone oil adheres to the obtained particles is an unavoidable problem. It seems that silicone oil KF-96-100CS to be convenient in the preparation of polymer particles. In comparison, we tried to use a much lower continuous phase than the pre-polymerization droplet's viscosity, namely toluene (0.56 mPa s). As a result, toluene is not suitable as a continuous phase and failed to prepare the polymer particles. Therefore, we noticed a

large difference in viscosity between pre-polymerization droplets and continuous phase is suggested to synthesize crosslinked poly(vinylphosphonic acid) particles through the W/O suspension polymerization method.

3.3.1.2 Effect of crosslinker

The hydroxyl moieties may be crosslinked with the monomers if partially hydrolyzed PVA is used as the stabilizer. In proportion to this statement, in this present study, we used the fully hydrolyzed stabilizer (PVA 99% hydrolyzed) to prevent such phenomena from occurring so that the PVA can sustain itself as a stabilizer ideally. However, the crosslinker concentration must be kept sufficiently low to obviate inter-particle bridging by crosslinking polymers occurring [29].

The synthetic yields of PVPA with varying PEGDA concentrations from 5% to 20% are shown in **Figure 3.2**. As a result, the synthetic yields were dependent on PEGDA content, whereas the synthetic yield increased as the concentration of the crosslinking agent increased. Tuncel [25], Kesenci [24], and Senel [30] found that the synthetic yield was affected by the concentration of crosslinking agent but not by agitation rate. Our results generally agree with these findings. In this study, however, the synthetic yield increased at a higher concentration of the PEGDA.

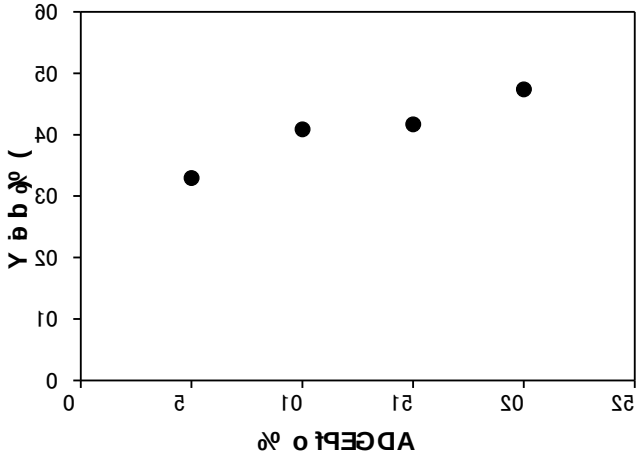

Figure 3.2. The effect of the crosslinking concentration on the PVPA-PEGDA yields.

3.3.2 Characterization

3.3.2.1 Fourier Transform-Infra Red (FT-IR) spectra

The infrared spectrum can be divided into three major regions: the far-infrared (less than 400 cm^{-1}), the mid-infrared (range between 4000 and 400 cm^{-1}), and the near-infrared (region 13000 – 4000 cm^{-1}). Many infrared applications employ the mid-infrared region, but the near- and far-infrared regions also provide essential information about specific materials and emphasize features of interest [31].

Figure 3.3 shows the FT-IR spectra of PVPA-PEGDA particles. The characteristic broad peak appearing between 3600 and 3100 cm^{-1} can be assigned to the O-H stretching of phosphonic acid groups of the PVPA. Band resulting from methylene asymmetric C-H stretching vibrations were observed at approximately 2960 cm^{-1}. However, these C-H stretching formed the shoulder around 2860 cm^{-1} by increasing the crosslinker content, known as C-H stretching symmetric. The different characteristics between methylene symmetric and asymmetric comprehensively discussed by Stuart [31].

The appearance of the multi-peak between 2160 and 1946 cm^{-1} and slightly broad peaks around 2600 – 2300 cm^{-1} were identified as P-OH stretching and hydrogen bonding

of P-OH surface among of phosphonic acid group in the polymer. Therefore, the peak intensity at this band increased with increasing PEGDA content. The phosphonic acid group gives the additional broadband in the 1625 cm^{-1}, which is merely seen for high crosslinking concentration. The peak at this band did not appear in PVPA-5, and the peak intensities increased with the increase in PEGDA content. This result is one assumption that increasing the amount of PEGDA increases the amount of phosphonic acid on the polymer particles. These results are also inclined with the increased yield by increasing the crosslinking agent, as explained in section **3.3.1.2**. Then, the carboxyl group (C=O) stretching vibration is seen at 1724 cm^{-1}, which is apparent for higher PEGDA content. Oppositely, this band does not significantly exist at lower PEGDA content in the polymer (in the case of PVPA-5). Moreover, the sharp peak at 1264 cm^{-1} indicating aliphatic P=O stretching from phosphonic acid functional groups. In addition to this, other supporting signs were also presented twin band at 1085-1000 cm^{-1} is attributed to P-O stretching. The FT-IR results provided strong evidence that PVPA-PEGDA particle was successfully synthesized.

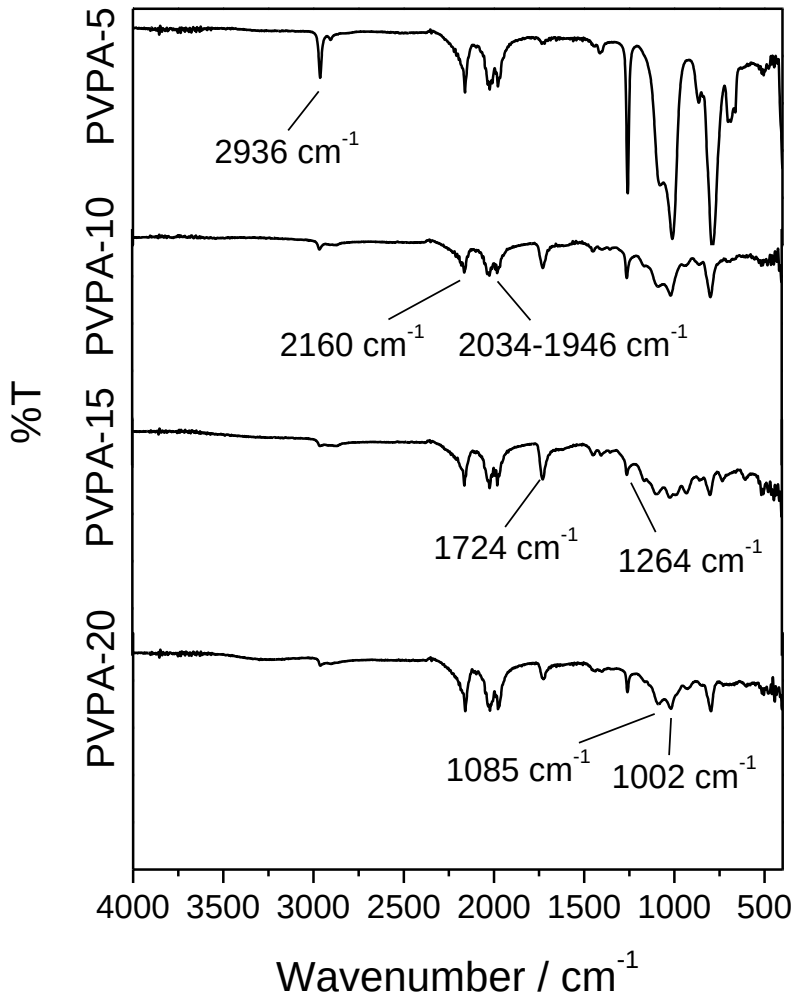

Figure 3.3. FT-IR spectra of PVPA-PEGDA particles.

After metal ion adsorption onto PVPA-10 particles, we recorded a low-intensity peak at 670 – 660 cm^{-1} and 457 cm^{-1}, mainly due to M-O bond formation's characteristic, as shown in **Figure 3.4**. Therefore, we conclude that IR results provide some outlook about the incorporation and complexation of metal ions with PVPA-10 particles.

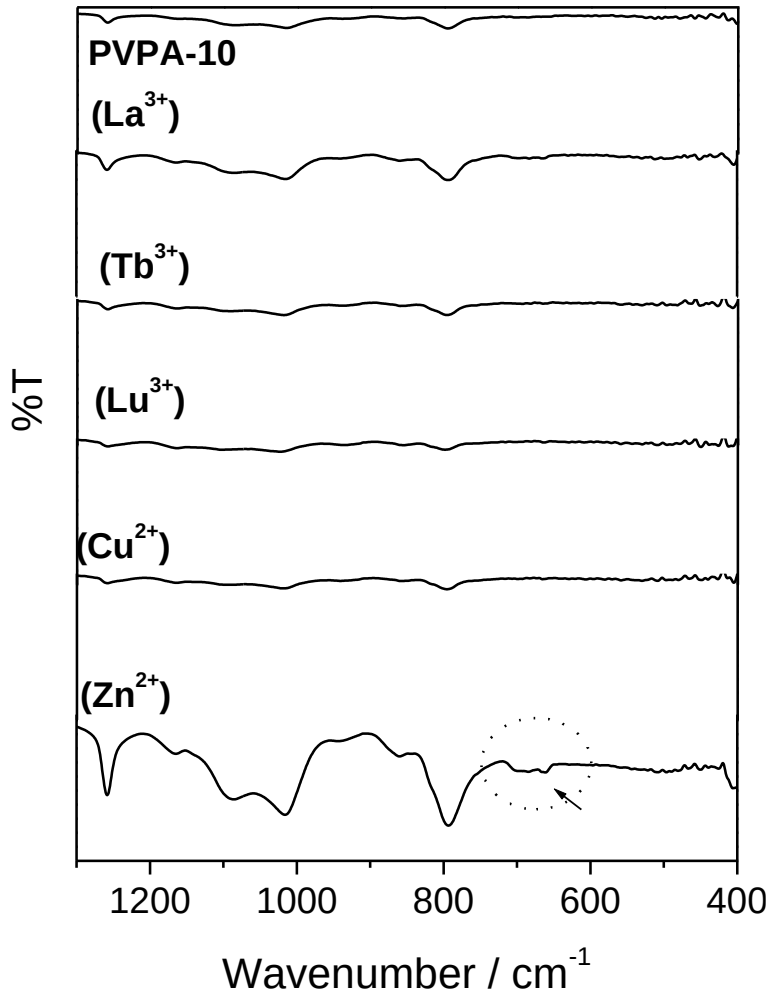

Figure 3.4. FT-IR spectra of PVPA-10 particle before and after metal ions adsorption.

3.3.2.2 Elemental analysis

The phosphorous content of the PVPA-10 particles was obtained by oxidative decomposition with mixed acid under elevated temperature. The phosphorous content was used to determine their functionalization degree. In this study, the phosphorous content in the PVPA-10 particles to be 3.08 wt% P. The degree of functionalization with phosphonic acid groups are relatively high, ensuring a sufficient for application as polymer-supported adsorbent in environmental separations, such as metal ion adsorption.

3.3.2.3 Particle morphology

For morphological evaluations, optical microscope and SEM images of PVPA with varying PEGDA content were obtained, illustrated in **Figure 3.5**. The optical microscope result reveals that the polymeric spherical particles with high polydispersity. The particles were spherical with sizes vary from 10 to 200 µm, irrespective of the components. On the others side, SEM images for PVPA-5 show the smooth surface morphology. However, the surface roughness becomes intense by increasing PEGDA content from 5% to 20%. This surface was wrinkled for all particles. In addition, the surface roughness of PVPA-20 is more than that of PVPA-5, which could be described by the existence of higher crosslinking content in PVPA-20 that affected the surface morphology.

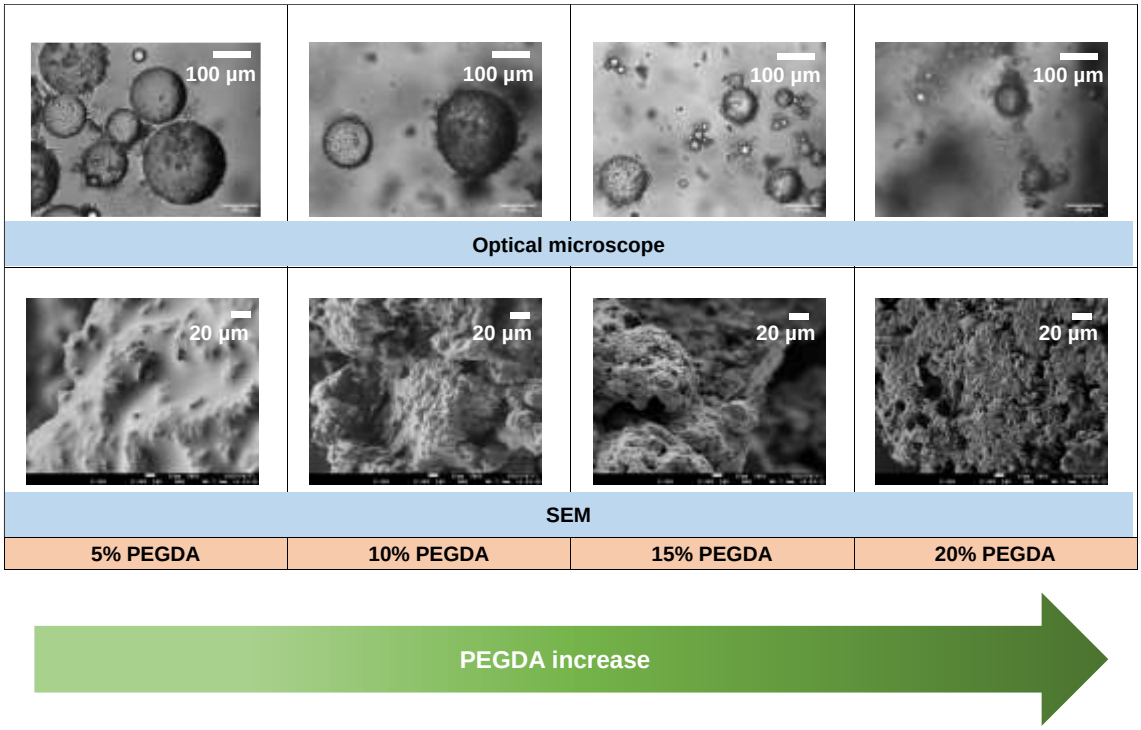

Figure 3.5. Optical microscope and SEM images of PVPA with varying PEGDA content. Scale bar corresponds to 100 µm for optical microscope and 10 µm for SEM images.

After metal ions adsorption, the particle surface was still able to maintain its wrinkles, but it had become smoother than before, as shown in **Figure 3.6**. The drying effect might

cause this phenomenon before use, where there are no more water molecules in the particles. Additionally, under careful investigation of the surface morphology of the metal ions-complexed PVPA-10 particle over a selected area, the SEM images depict the network- or pore-like surface. These conditions enable metal ions adsorbed onto PVPA-10 particles easily. However, we cannot recognize which part of the metal ion is adsorbed or distributed on the PVPA-10 surface.

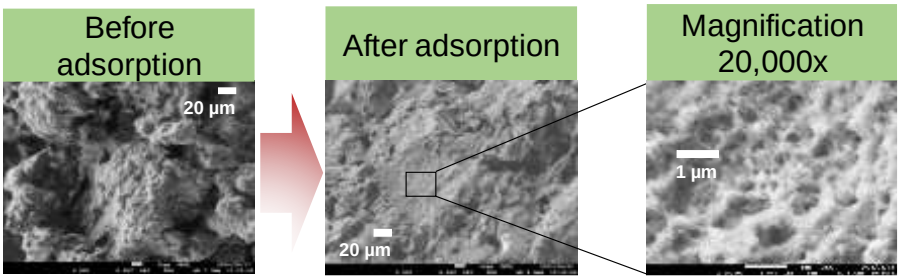

Figure 3.6. SEM images of PVPA-10 particle before and after La^{3+} ion adsorption. Scale bar corresponds to 10 µm and 1 µm for before/after adsorption and magnification 20k, respectively.

3.3.3 Metal ion adsorption studies

3.3.3.1 Effect of PEGDA content on metal ion adsorption

The effect of PEGDA content on Tb^{3+} percent extraction is depicted in **Figure 3.7**. The $\%E_A$ value increased from 21.30 % (q_e 0.91 x 10^{-3} ± 0.22 mmol g^{-1}) to 40.59 % (q_e 1.78 x 10^{-3} ± 0.33 mmol g^{-1}) when PEGDA content increases from 5 % to 10 % molar ratio with respect of VPA. As represented in SEM images, PEGDA affected the particles' surface morphology, such as surface roughness and pore size. As a result, at higher PEGDA content, continuous decreasing on the adsorption was observed. The q_e values observed for the samples PVPA-15 and PVPA-20 were 1.53 x 10^{-3} ± 0.17 mmol g^{-1} and 1.37 x 10^{-3} ± 0.24 mmol g^{-1}, respectively. At lower PEGDA content (PVPA-5), the $\%E_A$ is low due to the smooth adsorbent surface. Although, at higher PEGDA content (PVPA-15 and PVPA-20) shown, the $\%E_A$ is also low (33.49 % for PVPA-15 and 27.99 % for

PVPA-20) due to the larger number of filler/ polymer interactions restricted the network expansion. As a result, it is limited the liquid diffusion [32]. However, these values are higher than those of PVPA-5. These results indicate that rough surface is much better at adsorption than smooth surface polymer particles due to its liquid diffusion onto the pores. As the optimal composition, PVPA-10 gave the highest adsorption capacity of Tb^{3+} than the others (%E_A = 40.59 %), and it was used in the following experiments.

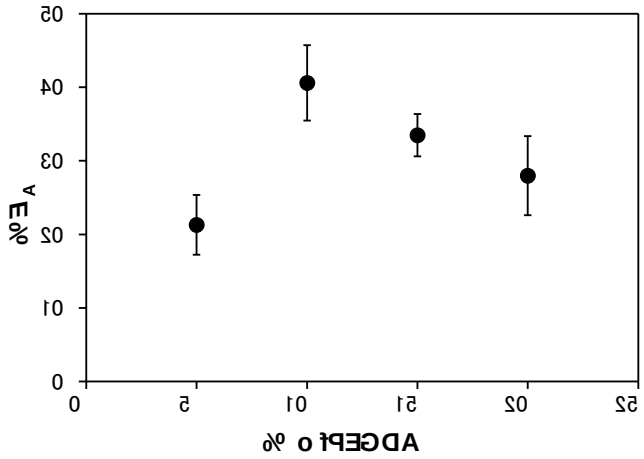

Figure 3.7. Effect of PEGDA content on Tb^{3+} percent extraction (Experimental condition: amount of adsorbent 20 mg; initial metal concentration 1 x 10^{-5} mol L^{-1}; volume 10 mL; pH 1.47~1.50; 300 rpm; room temperature; 60 min).

3.3.3.2 Effect of contact time on metal ions adsorption

Contact time is one of the most crucial parameters of adsorption to know the adsorption kinetics for an adsorbate solution with the given initial concentration. The amount of La^{3+}, Tb^{3+}, Lu^{3+}, Cu^{2+}, and Zn^{2+} ions adsorbed onto PVPA-10 particle has been determined at which increased with time until it attained a steady state after 240 – 720 min, and the results are presented in **Figure 3.8**.

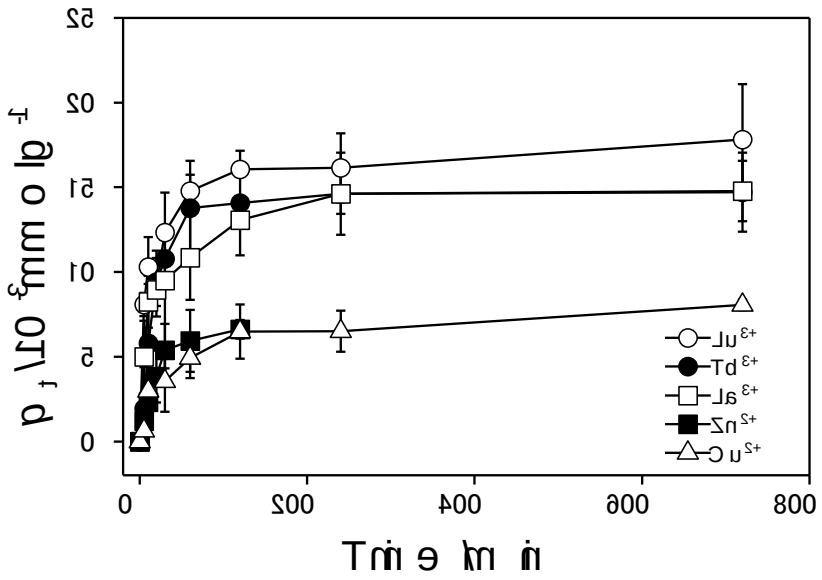

Figure 3.8. Effect of contact time on the amount of La^{3+}, Tb^{3+}, Lu^{3+}, Cu^{2+}, and Zn^{2+} ions adsorbed onto PVPA-10. (Experimental condition: amount of adsorbent 20 mg; initial metal concentrations 5 x 10^{-5} mol L^{-1}; volume 10 mL; pH 5.42; 300 rpm; room temperature).

It can be readily observed that sorption occurred faster in the first 30 min for all metal ions. This behavior can be referred to as the vacant active site on the PVPA-10 surface and high electrostatic attraction between metal ions and phosphonic acid functional groups. Other than that, the time to reach equilibrium is different for every metal ion. La^{3+} ions need more time to achieve the equilibrium condition as compare to others. Then, the adsorbed amount remains unchanged after 240 min, which indicates that the La^{3+} adsorption is nearly completed in 240 min. On the other side, a short time (120 min) is needed to reach equilibrium and become unchanged behind this point for Tb^{3+} and Lu^{3+} ions, respectively. Besides that, adsorption was most rapid for Lu^{3+} sorption onto PVPA-10 particles, followed by Tb^{3+} and La^{3+} ions. These results indicated that the time to reach equilibrium is progressively affected by the nature of metal ions in solution, i.e., ionic radii.

Furthermore, results disclosed that the lanthanide ions uptake follows the following arrangement: $Lu^{3+} > Tb^{3+} > La^{3+}$; the PVPA-10 particle shows maximum adsorption capacity toward Lu^{3+} and minimum for La^{3+}. Also, this uptake sequence is following the ionic radii; the ion with smaller ionic radii are easily distributed and move faster than the ions with greater ionic radii. To the best of our knowledge, the ionic radius for Lu^{3+} is 0.995 Å while Tb^{3+} is 1.090 Å and La^{3+} is 1.250 Å [33]. Lu^{3+} ion has smaller ionic radii, which is it would have high mobility to pass and distribute on the PVPA-10 surface active sites compared to those of Tb^{3+} and La^{3+} ions. Shortly reaction time, stable, and high adsorbed onto PVPA-10 particle were observed for Lu^{3+} because smaller ions became more convenient to diffuse and move. This performance designated that smaller metal ion's ionic radii can be uptake more quickly than the bigger one. Contrary condition for metal ions with greater ionic radii, difficulty to move, and low mobility and distribution may occur in the solution. As a result, the metal ions tend to be difficult to diffuse and adsorb onto the polymer surface.

Moreover, in the case of La^{3+} adsorption onto PVPA-10 particles, it is clear that the adsorption process is quite fast within the first 30 min. The amount of La^{3+} adsorbs onto PVPA-10 gradually increases until it remains unchanged after 240 min, which indicates that La^{3+} ion adsorption on PVPA-10 particles is nearly completed in 240 min. As a result, we can conclude that the optimal contact time for La^{3+} adsorption onto PVPA-10 is 240 min, and it was applied for the following experiments.

The amount of Tb^{3+} adsorb onto PVPA-10 particles at the contact time throughout 5 and 720 min was investigated. Contact time is express to influence the adsorption of Tb^{3+}, and the results clearly illustrate that the adsorption is initially quite fast within the first 30 min. This dealing was associated with the fast adsorption of Tb^{3+} on the PVPA-10 particle

due to fast diffusion and surface interactions. Then, the point is nearly approaching an equilibrium state within 120 min. After 120 min, the Tb^{3+} adsorb onto PVPA-10 particle slightly increases until 240 min and does not significantly improve with further contact time increases. In other words, the equilibrium was fully achieved after 240 min. Similar cases and tendencies are also valid for Lu^{3+} ions. Thus, the optimal contact time was chosen as 240 min for the following experiments.

We choose the most common and popular divalent metal ions in a comparison study on the adsorption process study, namely Cu^{2+} and Zn^{2+} metal ions. As we know, many researchers have been investigated and reported about adsorption behavior of divalent metal ions due to their stability in metal complexes formation. The amount of Cu^{2+} and Zn^{2+} ions adsorbed onto PVPA-10 particles is one-third lower than trivalent metal ions (La^{3+}, Tb^{3+}, Lu^{3+}). This result could be described by the effect of the electrostatic force difference of the metal ions. Trivalent metal ions possess high electrostatic interaction compared to that divalent metal ions to the active functional group on the PVPA-10 surface. Consequently, the attraction force for divalent metal ions is weaker than trivalent metal ions to active sites. As a result, the adsorption capacity of divalent metal ions is lower than trivalent metal ions.

3.3.3.3 Effect of initial solution pH on metal ions adsorption

Initial solution pH is one of the most critical factors controlling the adsorption process due to its substantial effects on ionization and the electrical charge of functional groups on the adsorbent surface [32][16]. The effects of initial solution pH on the adsorption capacity of trivalent metal (Ln^{3+} = La^{3+}, Tb^{3+}, and Lu^{3+}) and divalent metal (Cu^{2+} and Zn^{2+}) ions were investigated within the pH range between 1 and 6. Other parameters such

as contact time, amount of adsorbent, initial metal ions concentration, and temperature were kept constant at 240 min, 20 mg, 5 x 10^{-5} mol L^{-1}, and room temperature, respectively. The results revealed that the adsorption of La^{3+}, Tb^{3+}, Lu^{3+}, Cu^{2+}, and Zn^{2+} ions onto PVPA-10 surface was strongly pH-dependence. Higher pH values were not investigated for metal ions uptake to avoid the formation of metal hydroxides precipitation.

Figure 3.9 indicates that the amount of La^{3+}, Tb^{3+}, Lu^{3+}, Cu^{2+}, and Zn^{2+} ions uptake by PVPA-10 was remarkably enhanced when the initial solution pH increased from 1 to 6. This tendency holds true for all types of metal ions in this study. In order to explain this result, let us consider the recent work by Bingöl et al., [9] showed that PVPA behaves as a monoprotic acid, meaning that the second proton of monomer cannot be ionized in aqueous media. It was revealed that the charge density of a fully ionized PVPA chain would be unbearably high and thus prevent the second step in ionization [34]. They reported that almost linear increase of pH with α up to the nominal degree of neutralization of 0.5, which is achieved at pH around 6 or 7. Relying on this explanation, actually, PVPA already started deprotonated under this pH, however, not all the number phosphonate groups have been deprotonated yet. This is totally different from the parent monomer vinylphosphonic acid (VPA) behavior, which exhibits the expected two-step titration curve and possesses two pK_a values (2.74 and 7.34).

At low solution pH, protonation of a phosphonic acid functional group on the PVPA-10 surface occurred, making the surface of PVPA-10 positively charged. Thus, the PVPA-10's surface starts to repulse the cationic metal ions. Meanwhile, the metal ions compete with the high concentration of H^+ ions for the available adsorption sites on the PVPA-10. Consequently, the lower adsorption capacity of metal ions onto PVPA-10 was observed at a lower solution pH value.

Close to neutrality, the surface of PVPA-10 holds a negative charge due to the deprotonation of the surface functional group of PVPA-10. At this moment, a strong electrostatic interaction between cationic metal ions and anionic PVPA-10's surface could be ensured. For this reason, the metal ions adsorption capacity of the PVPA-10 improved up to pH 6. It is in good agreement with the results shown in **Figure 3.9.** Besides, the PVPA-10 had the best adsorption performance close to the pH of natural waters, which is a practical advantage since no treatment or adjusting is required before the adsorption process. The optimal pH for La^{3+}, Tb^{3+}, Lu^{3+}, Cu^{2+}, and Zn^{2+} adsorption on PVPA-10 was organized around 5 – 6.

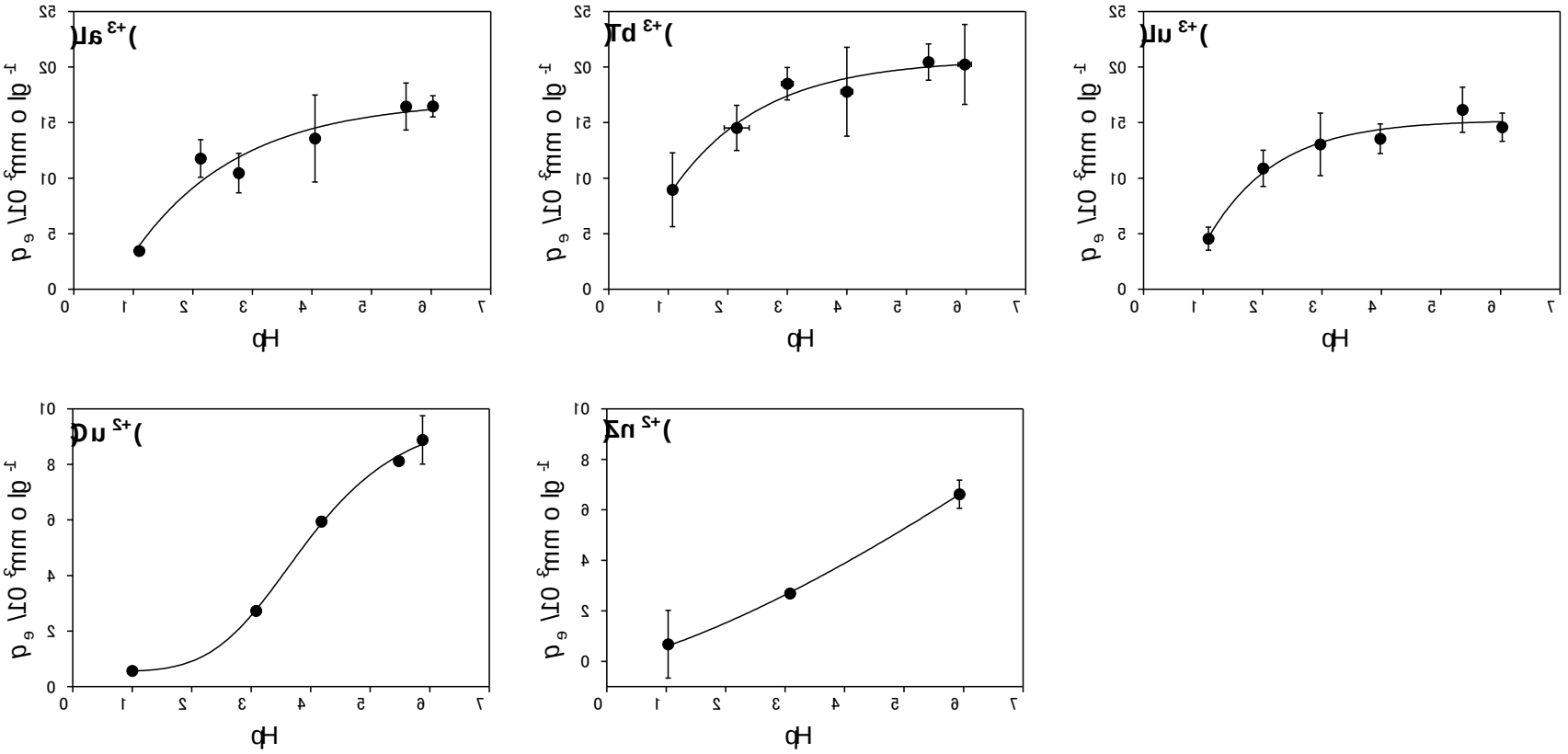

Figure 3.9. Effect of initial solution pH on La^{3+}, Tb^{3+}, and Lu^{3+}, Cu^{2+} and Zn^{2+}adsorption capacity (Experimental condition: amount of adsorbent 20 mg; initial metal concentration 5 x 10^{-5} mol L^{-1}; volume 10 mL; 300 rpm; room temperature; contact time 240 min for La^{3+}, Tb^{3+}, and Lu^{3+} and 120 min for Cu^{2+} and Zn^{2+}).

3.3.3.4 Effect of initial metal concentration on metal ion adsorption

The effect of initial metal concentration, C_0 (1 x 10^{-5} – 1 x 10^{-3} mol L^{-1}) on metal ion adsorption has been studied, and the results were depicted in **Figure 3.10**. The amount of metal ion adsorbed onto PVPA-10 particles increase when the initial metal concentration is increased and then remains constant till metal ions concentration of 5 x 10^{-4} mol L^{-1}. These findings were probably attributed to the higher driving force at elevated metal ion concentration, enhanced interaction between metal ions and PVPA-10 particles, and availability of a more functional site on the PVPA-10 surface [16][32][35][36]. Surprisingly, the lower amount of metal ions adsorbed at the low initial metal concentration due to not a strong enough driving force attacking the surface. Therefore, not all metal ions could bind to the active site of PVPA-10 particles. Then, the equilibrium adsorption capacity would be almost constant till metal ion concentration of up to 5 x 10^{-4} mol L^{-1}.

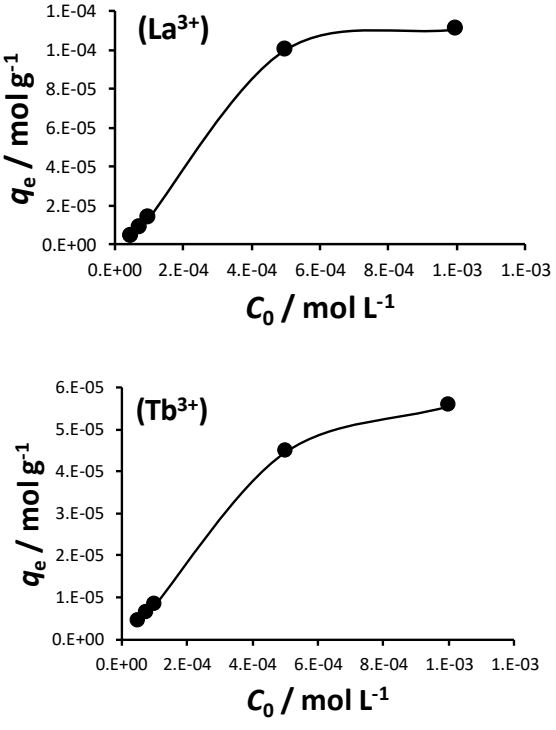

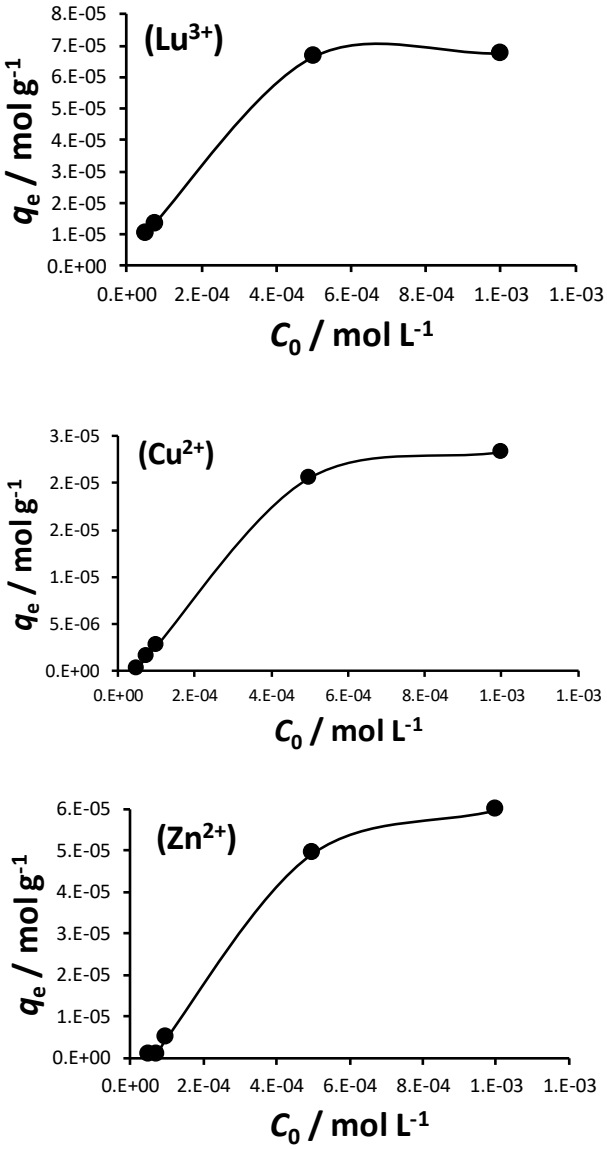

Figure 3.10. The effect of initial metal concentration on the amount of metal ions adsorbed onto PVPA-10 particles. (Experimental condition: amount of adsorbent 20 mg; volume 10 mL; pH 5 ~ 6; 300 rpm; room temperature; contact time 120 min).

3.3.3.5 Distribution ratio (*D*)

Distribution ratio (*D*) is the ratio of substance concentration in a single definite form in phase I to its concentration in the same form in phase II at equilibrium. Therefore, *D* is constant for one particular species under specified conditions only. In the current study,

we investigated the adsorption of metal ions in solution (liquid phase) on PVPA-10 particle (solid phase)

In section **3.3.3.3**, an obvious explanation about the adsorption of metal ions onto adsorbent is determined by pH dependence. It is clear that the adsorption of metal ions is generally small at low pH but increases with increasing pH above a specific condition, pH > p*K*a. The adsorption equilibrium can be represented by the following reaction:

$$M^{m+} + \overline{nL^-} + yCl^- \overset{K_{ad}}{\Longleftrightarrow} \overline{ML_nCl_y{}^{(m-n-y)+}}$$

Where species adsorbed on the solid are denoted by bars over characters and species in the solution phase are denoted by unbars. *M* is a metal ion, L^- is the available active site of the polymer, and Cl^- is anion from metal used in the experiment.

The distribution ratio (*D*) can be defined by the following relation:

$$\boldsymbol{D} = \frac{\left[\overline{\boldsymbol{ML_nCl_y{}^{(m-n-y)+}}}\right]}{[\boldsymbol{M^{n+}}]} = \frac{(\boldsymbol{C_0} - \boldsymbol{C_e})\ \boldsymbol{x}\ \boldsymbol{V/m}}{\boldsymbol{C_e}} \qquad \text{Equation 6}$$

Where C_0 is initial metal ion concentration (mol L^{-1}); C_e is residual metal ion concentration in solution (mol L^{-1}); V is the volume of aqueous phase (L); m is the mass of PVPA-10 used (g).

Adsorption constant (K_{ad}) can be defined by the following equation:

$$K_{ad} = \frac{\left[\overline{ML_nCl_y{}^{(m-n-y)+}}\right]}{[M^{m+}]\left[\overline{L^-}\right]^n[Cl^-]^y} \qquad \text{Equation 7}$$

The acid dissociation constant (K_a) can be expressed as follow:

$$K_a = \frac{[H^+][L^-]}{\left[\overline{HL}\right]} \qquad \text{Equation 8}$$

By substituting Eq.7 and Eq. 8 to Eq.6, a new form equation was obtained:

$$D = K_{ad}\left(\frac{K_a\left[\overline{HL}\right]}{[H^+]}\right)^n [Cl^-]^y \qquad \text{Equation 9}$$

$$\log D = \log K_{ad} {K_a}^n \left[\overline{HL}\right]^n [Cl^-]^y - \log[H^+]^n \quad \text{Equation 10}$$

Rearrangement Eq. 10 to obtain Eq.11 as follow:

$$\log D = \log K_{ad} {K_a}^n \left[\overline{HL}\right]^n [Cl^-]^y + n\ pH \quad \text{Equation 11}$$

At very dilute solution, coefficient activity is very small and can be neglected, then the symbol of $\log K_{ad} {K_a}^n \left[\overline{HL}\right]^n [Cl^-]^y$ is considered constant, thus Eq. 11 can be reduced in the following form:

$$\log D = n\ pH \quad \text{Equation 12}$$

The distribution ratio (*D*) helps estimate the distribution or partition of metal ions into solid in a solution. When the conditions of the adsorption process are fixed, the extraction equilibrium constant will rely on the ionic radii of the adsorbed metal ions and the ionic charge. The present study shows the partition of trivalent (Ln^{3+} = La^{3+}, Tb^{3+}, and Lu^{3+}) and divalent (Cu^{2+}, and Zn^{2+}) metal ions in solution onto PVPA-10 particle. To the best of our knowledge, when the valances of the Ln^{3+} ions are the same, the smaller the ionic radii of the Ln^{3+}, the more stable the adsorbed species and the bigger the distribution ratio (*D*) value. In the lanthanide series, the ionic radii of the elements decrease with increases in the atomic number. The equilibrium constant of extraction reactions, the stability of the complexes, and the distribution ratio all increase with the increase of the atomic number.

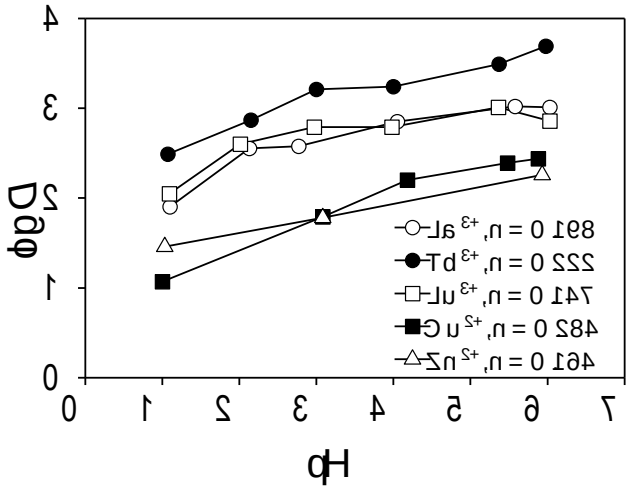

Figure 3.11. Log *D* of La^{3+}, Tb^{3+}, Lu^{3+}, Cu^{2+}, and Zn^{2+} ions against pH on PVPA-10 particles.

Figure 3.11 shown Log *D* against pH for La^{3+}, Tb^{3+}, Lu^{3+}, Cu^{2+}, and Zn^{2+} ions. We found that the log *D* values increase by increasing pH solution up to 6. In correlation to this study, it means a higher *D* value indicates more metal ions adsorbed onto PVPA-10 particles when the pH gradually increases. To the best of our knowledge, the higher the *D* values, the greater the substance's solubility. This finding will favor the higher metal uptake when it is close to neutrality, as previously discussed in the previous section. The results conclude here are similar to those reported in the literature for polyacrylamide stannic molybdophosphate as an organic-inorganic composite as a lanthanide ions adsorber [37].

It was observed that the dependency of log D values of all metal ions onto PVPA-10 particles on the pH of the solution. When log *D* against pH is plotted, a straight line with slope (n) is obtained. Slope (n) is referred to the valence of metal ions adsorbed. The linear relationship between log D and pH values was observed with a slope varying from 0.147 to 0.284. In fact, these slopes are not equal to the valence of metal ions adsorbed

onto PVPA-10 particles, which exhibit a non-ideal exchange reaction between metal ions and PVPA-10 particle surface. These findings cannot be explained only in terms of electrostatic interaction. Another consideration may be due to the formation of weakly acidic resin interaction; would be closely related to the ionic potential of the cations or the effect of different ionic radii.

3.3.4 Adsorption kinetic studies

To investigate the sorption mechanism and potential rate-controlling steps, kinetic models have been used to validate the experimental data. Several models can be used to express the mechanism of solute sorption onto a sorbent. These kinetic models were adequate to convey the sorption's characteristic constants, including the pseudo-first-order (PFO) and pseudo-second-order (PSO) kinetic models by Lagergren. These models have been widely used to describe adsorption rate in liquid-solid interaction, even under non-equilibrium conditions.

The PFO kinetic equation proposed by Lagergren [38] can be expressed as follows:

$$\frac{\mathbf{d}\boldsymbol{q_t}}{\mathbf{d}\boldsymbol{t}} = \boldsymbol{k_1}\ (\boldsymbol{q_e} - \boldsymbol{q_t}) \qquad \text{Equation 13}$$

By integrating this equation for the boundary conditions $t = 0$ to $t = t$ and $q_t = 0$ to $q_t = q_t$, Eq. 8 can be rearranged for linearized data plotting as shown by Eq. 9:

$$\ln\frac{(\boldsymbol{q_e} - \ \boldsymbol{q_t})}{\boldsymbol{q_e}} = \ -\boldsymbol{k_1 t} \qquad \text{Equation 14}$$

Elaborating Eq. 9, then the equation can be rewritten as follows:

$$\ln(\boldsymbol{q_e} - \boldsymbol{q_t}) - \ln \boldsymbol{q_e} = \ -\boldsymbol{k_1 t} \qquad \text{Equation 15}$$

$$\ln(\boldsymbol{q_e} - \boldsymbol{q_t}) = \ -\boldsymbol{k_1 t} + \ln \boldsymbol{q_e} \qquad \text{Equation 16}$$

Where q_e is the amount of metal ion adsorbed at equilibrium (mmol g^{-1}), q_t is the amount of metal ion adsorbed at specific contact time (mmol g^{-1}), k_1 is the rate constant for pseudo-first-order sorption (min^{-1}), and t is time (min).

Another model for the analysis of sorption kinetic is PSO. The kinetic rate law can be expressed as follows:

$$\frac{dq_t}{dt} = k_2(q_e - q_t)^2 \quad \text{Equation 17}$$

By integrating this equation for the boundary conditions $t = 0$ to $t = t$ and $q_t = 0$ to $q_t = q_t$, Eq. 12 can be rearranged for linearized data plotting as shown by Eq. 13:

$$\frac{1}{(q_e - q_t)} = \frac{1}{q_e} + k_2 t \quad \text{Equation 18}$$

Where k_2 is the pseudo-second-order rate constant, Eq. 13 can be rearranged to obtain a linear form:

$$\frac{t}{q_t} = \frac{1}{k_2 q_e^2} + \frac{1}{q_e} t \quad \text{Equation 19}$$

We summarized the kinetic models, their linear forms, and plot types to calculate the kinetic parameters of each model are shown in **Table 4**.

Table 4. The kinetic models, their linear forms, and plot types to calculate the kinetic parameters.

Kinetic Model	Linear Form	Plot	Parameters
PFO	$\ln(q_e - q_t) = \ln(q_e) - k_1 t$	$\ln(q_e\text{-}q_t)$ vs t	$\ln(q_e)$ = intercept $-k_1$ = slope
PSO	$t/q_t = 1/k_2 q_e^2 + 1/q_e t$	t/q_t vs t	q_e = 1/slope k_2 = slope^2/intercept

There is no problem in the linear form of PFO kinetic model-plotting ln ($q_e - q_t$) against t. However, using the linear form of the PSO kinetic model by plotting t/q_t against t must be conscientious about avoiding errors in describing the adsorption kinetics model.

Generally, this error is caused by entering the q_t value, which has reached the equilibrium condition. If we involve unchanged the q_t values with an increase in contact time, the calculation results will always reveal a straight line that refers to the PSO kinetic model. This finding agrees with Ho and McKay's review[39] that has analyzed many experimental results taken from the literature. They re-examined the published papers that were previously reported as a PFO kinetic model and concluded that the PSO kinetic model provides the best correlation of the experimental data for all the systems studied. This recommendation rests on the assumption that the adsorption process took place over a long time when the q_t value becomes constant due to equilibrium sorption conditions.

A PFO kinetic model was proposed to fit the experimental data well for an initial period of the first reaction step. The same thing was also stated by Simonin et al. [40] that explained the tendency PFO kinetic model is better to describe the experimental data than the PSO kinetic model for the initial period before the adsorption reaches the equilibrium. Experimental evidence was also reported by Lee et al. [41] for the dye adsorption onto TiO_2 surface at the short time in contact time. After the equilibrium condition, as mentioned above, the PSO kinetic model is probably more appropriate to describe the data than the PFO model. *Simonin* has clearly explained the rebuttal about Ho and McKay's literature review.

To point out that the PFO kinetic model is better described for an initial period of the first reaction step than the PSO kinetic model at the same time. However, it seems that the PSO kinetic model cannot quite well account for such a process because it cannot represent the step rise of the adsorption at short times.

Dealing with the misinterpretation in determining the kinetic model, the calculation is analyzed at a short time, indicating the step rise of the adsorption for either PFO or

PSO kinetic model. The kinetics model analysis of the adsorption rate of La^{3+}, Tb^{3+}, Lu^{3+}, Cu^{2+}, and Zn^{2+} ions onto PVPA-10 particles was carried out within a bit of contact time. This analysis is carried out when there is a significant change in the absorption of La^{3+}, Tb^{3+}, Lu^{3+}, Cu^{2+}, and Zn^{2+} ions just before an equilibrium state is reached. The linear plot type result is shown in Figures **3.12** and **3.13,** and their kinetic parameters are summarized in **Table 5**. Our system fits either PFO or PSO kinetic model best according to the correlation coefficient (R^2) values. Since the R^2 values are enough high for both kinetic model, indicate good fit between the data and the model[42], but not guarantee the model acceptability. However, because the R^2 is not a sufficient criterion[43] and the criterion for choosing the suitable model does not rely solely on R^2, the residues resulting from a fit are needed to exhibit a random behavior around zero as a function of time.

The figures below summarize the R^2 value for the linear plots of $\ln(q_e - q_t)$ against t from the PFO kinetic model and plot t/q_t against t from the PSO kinetic model. All systems are determined just before reaching equilibrium sorption.

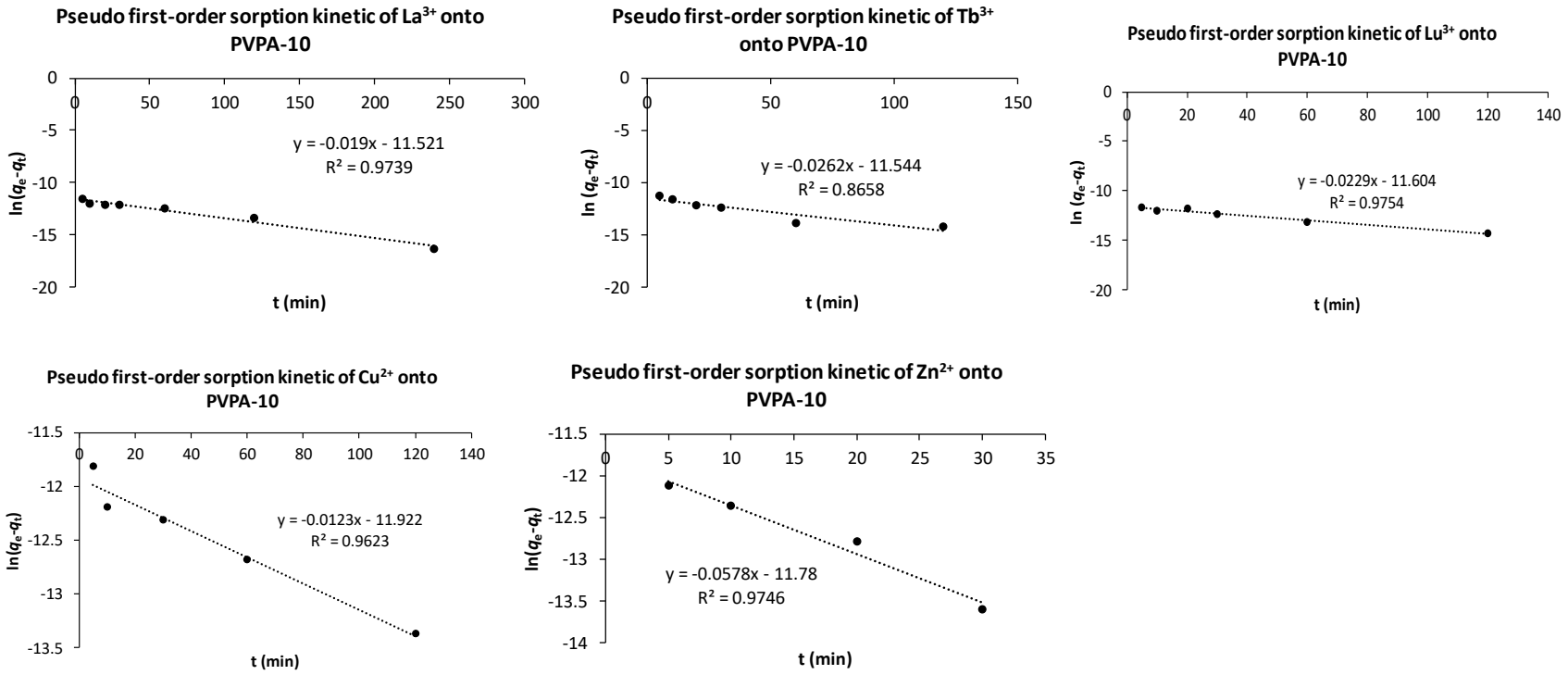

Figure 3.12. Linear plot $\ln(q_e - q_t)$ against t for PFO kinetic model of metal ions.

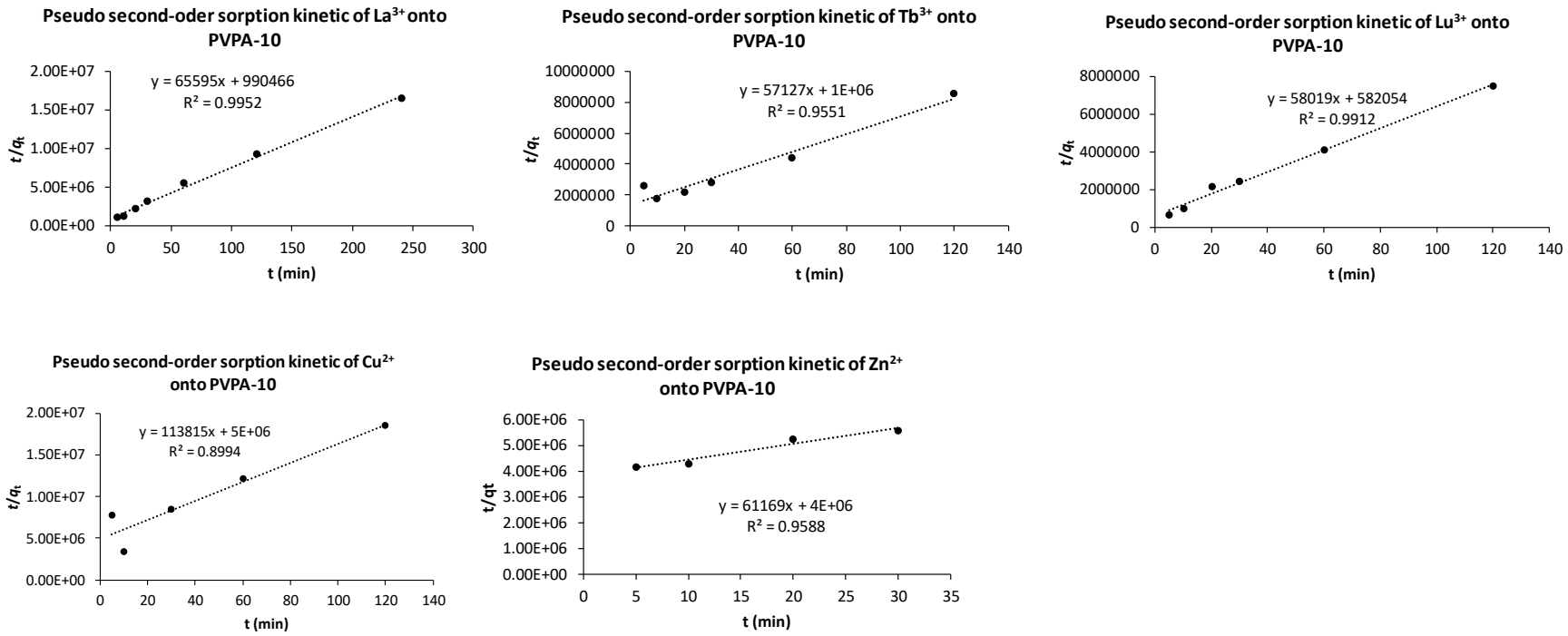

Figure 3.13. Linear plot t/q_t against t for PSO kinetic model of metal ions.

Table 5. Kinetic parameters of PFO and PSO for La^{3+}, Tb^{3+}, Lu^{3+}, Cu^{2+}, and Zn^{2+}.

Metal ion	C_0 / 10^{-5} mol L^{-1}	$q_{e,\,exp}$ / 10^{-3} mmol g^{-1}	PFO			PSO		
			$q_{e,\,calc}$ / 10^{-3} mmol g^{-1}	k_1 / min^{-1}	R^2	$q_{e,\,calc}$ / 10^{-3} mmol g^{-1}	k_2 / M^{-1} min^{-1}	R^2
La^{3+}	5	14.69	9.92	0.019	0.9739	15.24	4344.12	0.9952
Tb^{3+}		14.70	9.70	0.0262	0.8658	17.50	3263.50	0.9551
Lu^{3+}		16.68	9.13	0.0229	0.9754	17.24	5783.32	0.9912
Cu^{2+}		8.05	6.64	0.0123	0.9623	8.79	2590.77	0.8894
Zn^{2+}		6.62	7.66	0.0578	0.9746	16.35	935.41	0.9588

We should evaluate the residues or linear modeling adsorption kinetics errors using different validation methods to avoid the spurious conclusion. These validation methods including Sum of Square Error (SSE), Chi-Square (χ^2), Mean Square Error (MSE), Root Means Square Error (RMSE), Normalized Standard Deviation (Δy(%)), Average Relative Error (ARE), and Sum of Absolute Error (SAE). Unfortunately, this vital step is quite often overlooked or given lesser importance. However, some researchers have combined these model validation methods and R^2 to determine the best-fitting kinetic model. Wu et al. [44] tried to use Normalized Standard Deviation (Δy(%)) to evaluate the adsorption data from dyes and Cu^{2+} on chitosan. Lin et al. [45] and Tan et al. [46] combined R^2 and q_e value with Δy(%) to ensure the adsorption kinetic model of dyes onto activated carbon.

Moreover, Xiao et al. [47] evaluated experimental adsorption data and inspected the residual plot to determine the goodness of fit of their work. Currently, Aziz et al. [48] have been reported using combination SSE, χ^2, and Δy(%) to testing the error of the linearized adsorption data. All the mentioned published reports above conclude that R^2 is not enough to conclude the adsorption kinetic models. To address these challenges, model validation methods are used to determine a suitable kinetic model. Each of these validation methods is a measure of how low the model error is. Consequently, the model that fits a datasheet would have R^2 closer to unity and lower values of the other validation methods. The detailed calculation will discuss in section **3.3.5**

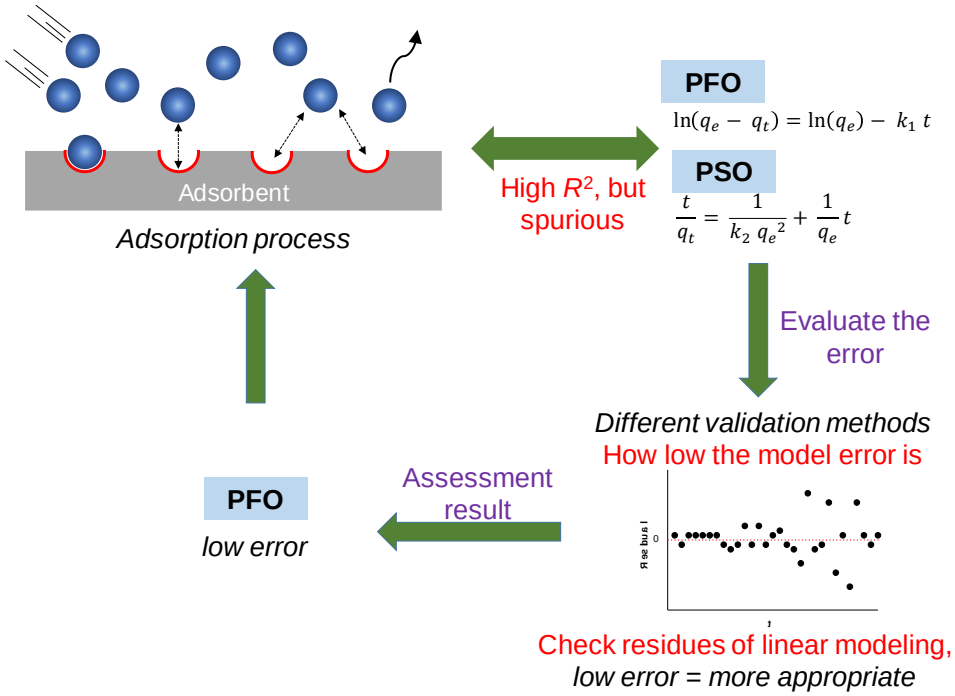

Figure 3.14. Representation of the framework of thinking to avoid the spurious conclusion in determining a suitable kinetic model.

3.3.5 Evaluation of kinetic models using different validation methods

As indicated above, the evaluation of experimental data could be applied using different validation methods. The fitting validity of these models can be checked by each linear plot of $\ln(q_e - q_t)$ against t and t/q_t against t for PFO and PSO kinetic model, respectively. The validation methods and their formula are represented in **Table 6.** All the result is to minimize the model error. The lower the model error, the lower the values of the validation methods, except for R^2, which gets closer to unity. **Table 7** summarizes the assessment results for validation methods. Calculated values for all validation methods are lower for PFO than PSO kinetic model. Based on this calculation, we could say that La^{3+}, Tb^{3+}, Lu^{3+}, Cu^{2+}, and Zn^{2+} ions adsorbed onto PVPA-10 are better described by PFO rather than PSO kinetic model.

Table 6. Validation methods to evaluate the experimental adsorption data.

Validation Method	Equation	Eq. No
Coefficient of Correlation, R^2	$R^2 = 1 - \frac{\sum_{i=1}^{n}(y_{exp} - y_{calc})^2}{\sum_{i=1}^{n}(y_{exp} - \bar{y}_{exp})^2}$	Equation 20
Sum of Square Error, SEE	$SSE = \sum_{i=1}^{n}(y_{exp} - y_{calc})^2$	Equation 21
Chi-Square, χ^2	$\chi^2 = \sum_{i=1}^{n}\frac{(y_{exp} - y_{calc})^2}{y_{calc}}$	Equation 22
Mean Square Error, MSE	$MSE = \frac{1}{n}\sum_{i=1}^{n}(y_{exp} - y_{calc})^2$	Equation 23
Root Mean Square Error, RMSE	$RMSE = \sqrt{\frac{1}{n}\sum_{i=1}^{n}(y_{exp} - y_{calc})^2}$	Equation 24
Normalized Standard Deviation, Δy (%)	$\Delta y\ (\%) = \sqrt{\frac{1}{n-1}\sum_{i=1}^{n}\left(\frac{y_{exp} - y_{calc}}{y_{exp}}\right)^2}\ x\ 100$	Equation 25
Average Relative Error, ARE	$ARE = \frac{1}{n}\sum_{i=1}^{n}\left\lvert\frac{y_{exp} - y_{calc}}{y_{exp}}\right\rvert$	Equation 26
Sum of Absolute Error, SAE	$SAE = \sum_{i=1}^{n}\lvert y_{exp} - y_{calc}\rvert$	Equation 27

Table 7. Overall evaluation of different validation methods for linearized adsorption kinetic model of PFO and PSO for La^{3+}, Tb^{3+}, Lu^{3+}, Cu^{2+}, and Zn^{2+} ions.

Validation Method	La^{3+}		Tb^{3+}		Lu^{3+}		Cu^{2+}		Zn^{2+}	
	PFO	**PSO**	**PFO**	**PSO**	**PFO**	**PSO**	**PFO**	**PSO**	**PFO**	**PSO**
R^2	0.9739	0.9952	0.8658	0.9551	0.9754	0.9912	0.9623	0.8994	0.9746	0.9588
$q_{e,\,calc}$ / 10^{-3} mmol g^{-1}	9.92	15.24	9.70	17.50	9.13	17.24	6.64	8.79	7.66	16.35
SSE	0.4222	8.98E+11	0.9985	2.19E+12	0.1246	2.82E+11	0.0524	1.29E+13	0.0321	1.88E+11
χ^2	-0.0314	2.98E+4	-0.0767	1.4E+6	-0.0101	2.06E+5	-0.0043	2.18E+06	0.0025	3.82E+04
MSE	0.0603	1.2E+11	0.1664	3.65E+11	0.0208	4.70E+10	0.0105	2.58E+12	0.008	4.72E+10
RMSE	0.2456	3.58E+5	0.4079	6.04E+5	0.1441	2.17E+5	0.1024	1.61E+06	0.0896	2.17E+5
Δy(%)	2.0043	20.3	3.3665	23.2	1.2845	22.12	0.9543	4.39E+01	0.8027	5.42
ARE	0.0162	1.33E-1	0.0254	0.7201	0.0101	0.1417	0.0064	2.31E-01	0.0056	0.0387
SAE	1.4832	2.24E+6	1.9757	2.29E+6	0.7511	1.03E+6	0.3855	5.55E+06	0.2906	7.19E+5

n = 7, 6, 6, 5, and 4 for La^{3+}, Tb^{3+}, Lu^{3+}, Cu^{2+} and Zn^{2+}, respectively.

$q_{e,\,exp}$ / 10^{-3} mmol g^{-1} = 14.69, 14.70, 16.68, 8.05, and 6.62 for La^{3+}, Tb^{3+}, Lu^{3+}, Cu^{2+} and Zn^{2+}, respectively.

3.3.6 Adsorption isotherm studies

The equilibrium adsorption isotherm reveals that there are interactions between the adsorbents and metal ion molecules when the adsorption process reaches equilibrium. An adsorption isotherm expresses the relationship between the adsorption capacity (q_e) and equilibrium concentration (C_e) of the adsorbate. Both the Freundlich and Langmuir`s non-linear models were evaluated for description of metal adsorption isotherm, due to its more accurate results than a linear equation. The non-linear of Freundlich and Langmuir models are expressed in **Equation 28** and **29**:

$$q_e = K_F C_e^{\,1/n} \qquad \text{Equation 28}$$

$$q_e = \frac{q_m K_L C_e}{1 + K_L C_e} \qquad \text{Equation 29}$$

Where q_e is the amount of metal ion adsorbed at equilibrium (mmol g^{-1}), C_e is equilibrium metal ion concentration at specific contact time in solution (mol L^{-1}), 1/n is the dimensionless adsorption intensity of the Freundlich model which indicates the heterogeneity factor ($0 \geq 1/n \leq 1$). K_F and K_L are the Freundlich and Langmuir constants, respectively, and q_m is the maximum adsorption capacity (mmol g^{-1}).

The main difference between these two models is that Freundlich model assumes that an adsorption process on heterogeneous surfaces with different affinities that have multilayer adsorption, whereas the Langmuir model assumes that metal ions are adsorbed as a monolayer on the adsorbent surface.

The experimental adsorption isotherms are shown in **Figure 3.15**, and all of the constants obtained from the experimental data are listed in **Table 8**. The Freundlich constant (K_F) and 1/n were calculated from the plot of q_e against C_e using **Equation 28**; the Langmuir constant (K_L) and q_m were obtained from the plot of q_e against C_e using **Equation 29**.

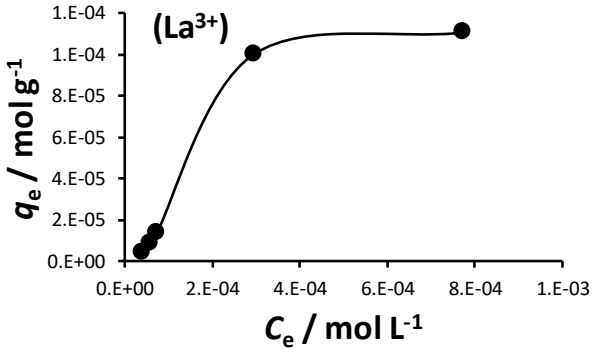
(La3+)
1.E-04
1.E-04
8.E-05
6.E-05
4.E-05
2.E-05
0.E+00
qe / mol g-1
0.E+00
2.E-04
4.E-04
6.E-04
8.E-04
1.E-03
Ce / mol L-1

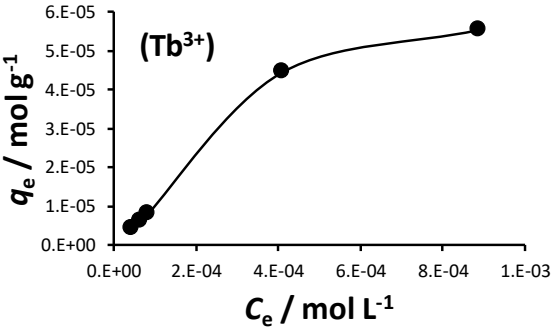
(Tb3+)
6.E-05
5.E-05
4.E-05
3.E-05
2.E-05
1.E-05
0.E+00
qe / mol g-1
0.E+00
2.E-04
4.E-04
6.E-04
8.E-04
1.E-03
Ce / mol L-1

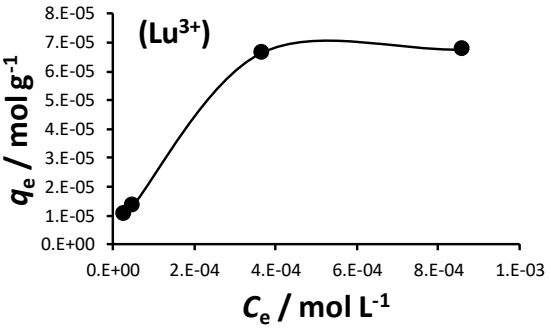
(Lu3+)
8.E-05
7.E-05
6.E-05
5.E-05
4.E-05
3.E-05
2.E-05
1.E-05
0.E+00
qe / mol g-1
0.E+00
2.E-04
4.E-04
6.E-04
8.E-04
1.E-03
Ce / mol L-1

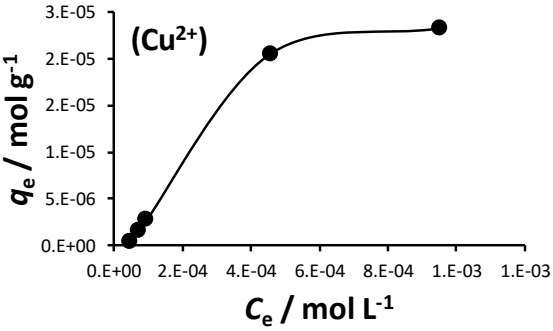
(Cu2+)
3.E-05
2.E-05
2.E-05
1.E-05
5.E-06
0.E+00
qe / mol g-1
0.E+00
2.E-04
4.E-04
6.E-04
8.E-04
1.E-03
1.E-03
Ce / mol L-1

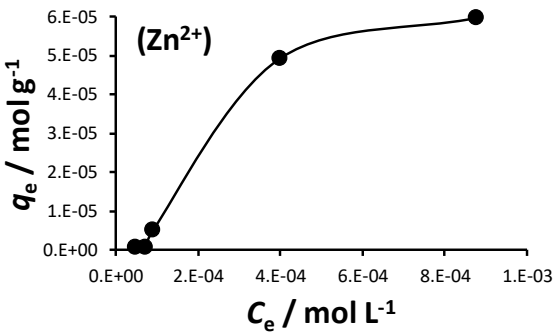

Figure 3.15. Adsorption isotherms of metal ions by PVPA-10 particles. (Experimental condition: amount of adsorbent 20 mg; volume 10 mL; pH 5 ~ 6; 300 rpm; room temperature; contact time 120 min).

Table 8. Isotherm constant for the adsorption of metal ions onto PVPA-10 particles.

	Langmuir model			**Freundlich model**		
Metal ion	q_m / mmol g^{-1}	K_L / L mol^{-1}	R^2	K_F / L g^{-1}	1/n	R^2
La^{3+}	0.185	2357.6	0.89643	0.00665	0.56	0.98761
Tb^{3+}	0.097	1640.1	0.97462	0.00419	0.60	0.99078
Lu^{3+}	0.088	5515.6	0.96285	0.00106	0.37	0.96297
Cu^{2+}	0.045	1260.7	0.93493	0.00459	0.75	0.89541
Zn^{2+}	0.135	999.1	0.91884	0.00904	0.70	0.99557

3.3.7 Mechanism of metal ion adsorption

As mention at the beginning of this chapter, adsorption of trivalent metal ions had not been extensively studied as that of divalent metal ions. Consequently, there is no detailed report that has been discussed about the mechanism of the adsorption for trivalent metal ions. Some researchers briefly reported about the adsorption process, but there is no detail about the mechanism as published by [49][50][51]. To address this challenge, we

proposed the foremost mechanism on the adsorption of trivalent metal ions and divalent metal ions onto PVPA-10 particles. The PVPA-10 particle possesses a phosphonic acid functional group on its surface, which can be negatively or positively charged depending on its environmental conditions, as inferred in section **3.3.3.2**. Relying on this assumption and other experimental results, we proposed that the primary mechanism of sorption of metal ions onto PVPA-10 particles occurs in two ways: (1) ion exchange and (2) adsorption.

Although these two mechanisms share similar characteristics, ion exchange is known as a bulk phenomenon that involves the entire volume of the adsorbent, while adsorption is typically a surface phenomenon [36]. At low solution pH, the surface of PVPA-10 holds positively charged. Therefore, metal ions binding predominant mode is ion-exchange through exchange between H^+ of a phosphonic acid functional group on the adsorbent surface and metal ions. However, at high solution pH, the surface of PVPA-10 holds a negative charge due to the deprotonation of the surface functional group of PVPA-10. Since it possesses a negative charge surface of PVPA-10, cationic metal ions get attracted and finally get adsorbed onto the PVPA-10 surface. We summarize that the metal ions uptake occurs either by ion exchange or adsorption or by both, depending on the charged state of the adsorbent surface, as shown schematically in **Figure 3.16**.

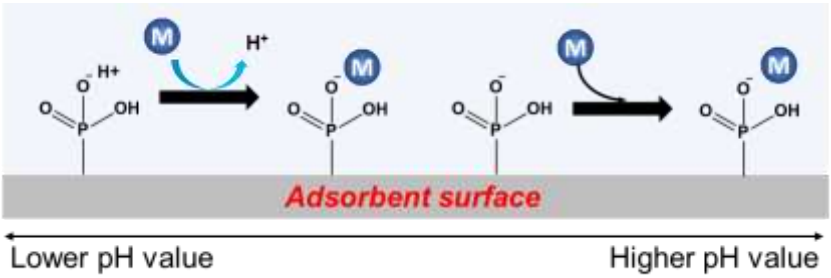

Figure 3.16. Schematic representation of two different mechanisms of metal ions uptake through ion exchange and adsorption at different pH values.

We also tried to discuss the coordination mode between the phosphonic acid functional group on the PVPA-10 surface and metal ions. The phosphonic acid group can act adequately as a chelate that allows the exchanging of metal ions. Yuchi et al. reported two coordination modes of trivalent metal ions on chelating resin containing iminodiacetic acid groups [11]. In this study, we adopted this coordination mode containing phosphonic acid functional group on the polymer surface. In principle, these coordination modes including (1) all three donor atoms from phosphonic acid functional groups coordinates to metal ions, and (2) two donor atom from phosphonic acid functional groups coordinates to metal ions, as shown in **Figure 3.17**.

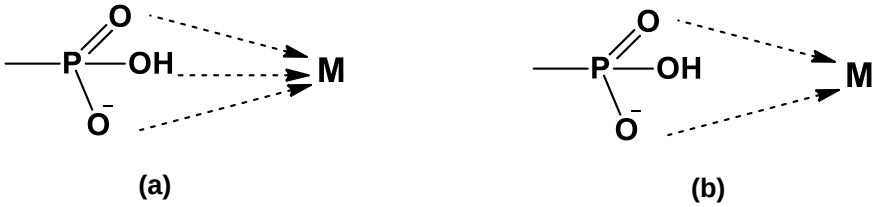

Figure 3.17. Illustration of two different coordination modes: (a) all three donor atoms from phosphonic acid functional groups coordinates to metal ions, and (b) two donor atoms from phosphonic acid functional groups coordinates to metal ions (M= M^{3+} or M^{2+}).

If PFO kinetic model holds true, these mechanisms and coordination mode are fluently acceptable. In the PFO kinetic model, one metal ion exclusively adsorbed onto one unoccupied active site. This result means, one active site on the polymer surface would interact with one metal ion simultaneously. These findings are to be inclined with the experimental results in sections **3.3.3.2** and **3.3.4.**

3.3.8 Comparison of sorption properties with other sorbents

Table 9 reports La^{3+}, Tb^{3+}, Lu^{3+}, Cu^{2+}, and Zn^{2+} adsorption capacities of different sorbents. The experimental conditions are not systematically identical (making thus the strict

comparison difficult) and lack publications on adsorption of these metals using functionalized polymers. These data demonstrate that PVPA-10 has comparable sorption capacities for La^{3+}, Tb^{3+}, Lu^{3+}, Cu^{2+}, and Zn^{2+} than most reported pieces of literature and other functional groups such as carboxylic acid, sulfonic acid, and amide. However, our synthesized polymer is shown outstanding performance as compared to several publications that have been reported.

Table 9. Comparison of La^{3+}, Tb^{3+}, Lu^{3+}, Cu^{2+}, and Zn^{2+} adsorption capacities for selected sorbents.

Adsorbent	q_{max} (mmol g^{-1})					Time (min)	Reference
	La(III)	Tb(III)	Lu(III)	Cu(II)	Zn(II)		
Poly(acrylic acid)-functionalized montmorillonite	2.020	-	-	-	-	60	[52]
Carboxylic acid-functionalized diatomite	1.004	-	-	-	-	20	[53]
Poly(hydroxamic acid)-functionalized polystyrene	1.270					210	[54]
Microalgae biosorbent	0.720	-	-	-	-	360	[55]
Nitrolite	0.034	-	-	-	-	1440	[51]
Poly(acrylic acid) grafted onto silica hydrogels	1.675	0.157	-	-	-	180	[56]
Bicine functionalized amberlite XAD-4 resin	0.35	0.42	-	-	-	30	[57]
DTPA-functionalized magnetic nanoadsorbent	6.551 x 10^{-7}	8.822 x 10^{-6}	-	-	-	30	[58]
Phosphonate-based alginate-polyethylenimine	0.46	0.37	-	-	-	2880	[59]
Polyacrylamide-functionalized natural zeolite	-	0.32	-	-	-	600	[60]
Polyacrylamide-functionalized synthetic zeolite	-	0.66	-	-	-	600	[60]
2-thenoyltrifluoroacetine supported onto polyurethane foam	-	0.042	-	-	-	5	[61]
DOTP-based hydroxyapatite	-	0.024	-	-	-	5	[62]
MePhPTA-functionalized alumina-silica	-	-	0.742	-	-	60	[63]
Diamide grafted onto mesoporous silica	-	-	0.042	-	-	120	[64]
Sulfonic acid-functionalized nonporous silica	-	-	-	4.091	-	120	[65]
Acrylic acid and crotonic acid-functionalized Fe_3O_4 magnetic nanoparticles	-	-	-	0.977	0.603	45	[66]

Aminosalicylic acid grafted onto PGMA-SiO_2	-	-	-	0.420	0.350	120	[67]
Xanthate-modified magnetic chitosan	-	-	-	0.544	0.318	-	[68]
Phosphonic acid-functionalized particles	0.185	0.097	0.088	0.045	0.135	120	*This work*

3.4 Summary

In this chapter, the crosslinked poly(vinylphosphonic acid) particles were successfully synthesized by the water-in-oil (W/O) suspension polymerization method, and their adsorption properties were investigated. PEGDA as crosslinker was varied from 5 to 20 % molar ratio concerning VPA content to generate PVPA-5, PVPA-10, PVPA-15, and PVPA-20 polymer particles. In the preliminary study, PVPA-10 particles gave the highest adsorption capacity of Tb^{3+} than the others, which were then chosen as an adsorbent for metal ions adsorption. FT-IR confirmed the structures of the particles, and SEM and optical microscope examined the morphology of the particles. Obtained particles shown high polydispersity with their size ranged from 10 to 200 μm.

A batch adsorption experiment was employed to trivalent (La^{3+}, Tb^{3+}, and Lu^{3+}) and divalent (Cu^{2+} and Zn^{2+}) metal ions adsorption onto PVPA-10 particles. The adsorption performance showed good pH-dependent due to charged state of the adsorbent surface. The adsorption kinetics was best described by either PFO or PSO kinetic model according to correlation coefficient (R^2) values, which are high enough for both kinetic models. However, the R^2 value does not guarantee the model acceptability. Therefore, to avoid the spurious conclusion, the residues resulting from a linear fit kinetic model should be evaluated using other validation methods and exhibit how low the model error is. Based on this calculation, we could say that La^{3+}, Tb^{3+}, Lu^{3+}, Cu^{2+}, and Zn^{2+} ions adsorbed onto PVPA-10 are better described by PFO rather than PSO kinetic model. However, from the viewpoint of chemical reaction, PFO kinetic model is more reasonable to explain the reaction mechanism since one metal ion is exclusively adsorbed onto one unoccupied adsorption active site.

Non-linear Freundlich and Langmuir isotherm models were used to represent the

experimental data. The maximum adsorption of La^{3+}, Tb^{3+}, Lu^{3+}, Cu^{2+}, and Zn^{2+} predicted using Langmuir adsorption isotherm model to be 0.185, 0.097, 0.088, 0.045, and 0.135 mmol g^{-1}, respectively.

3.5 References Chapter III

[1] B. Valerie, Alard., Garbine, Aguirre., Laurent, "Microgels for the delivery of cosmetic active organic substances," 2019.

[2] R. E. Dey, I. Wimpenny, J. E. Gough, D. C. Watts, and P. M. Budd, "Poly(vinylphosphonic acid-co-acrylic acid) hydrogels: The effect of copolymer composition on osteoblast adhesion and proliferation," *J. Biomed. Mater. Res. - Part A*, vol. 106, no. 1, pp. 255–264, 2018, doi: 10.1002/jbm.a.36234.

[3] J. A. Bonham, M. A. Faers, and J. S. Van Duijneveldt, "Non-aqueous microgel particles: Synthesis, properties and applications," *Soft Matter*, vol. 10, no. 47, pp. 9384–9398, 2014, doi: 10.1039/c4sm01834f.

[4] Z. Dai and T. Ngai, "Microgel particles: The structure-property relationships and their biomedical applications," *J. Polym. Sci. Part A Polym. Chem.*, vol. 51, no. 14, pp. 2995–3003, 2013, doi: 10.1002/pola.26698.

[5] R. A. Meurer *et al.*, "Biofunctional Microgel-Based Fertilizers for Controlled Foliar Delivery of Nutrients to Plants," *Angew. Chemie - Int. Ed.*, vol. 56, no. 26, pp. 7380–7386, 2017, doi: 10.1002/anie.201701620.

[6] K. Naseem, Z. Hussain Farooqi, M. Zia Ur Rehman, M. Atiq Ur Rehman, and M. Ghufran, "Microgels as efficient adsorbents for the removal of pollutants from aqueous medium," *Rev. Chem. Eng.*, vol. 35, no. 2, pp. 285–309, 2019, doi: 10.1515/revce-2017-0042.

[7] M. Ahmaruzzaman, "Industrial wastes as low-cost potential adsorbents for the treatment of wastewater laden with heavy metals," *Adv. Colloid Interface Sci.*, vol. 166, no. 1–2, pp. 36–59, 2011, doi: 10.1016/j.cis.2011.04.005.

[8] B. L. Rivas, E. Pereira, P. Gallegos, D. Homper, and K. E. Geckeler, "Metal ion

binding capability of the water-soluble poly(vinyl phosphonic acid) for mono-, di-, and trivalent cations," *J. Appl. Polym. Sci.*, vol. 92, no. 5, pp. 2917–2922, 2004, doi: 10.1002/app.20246.

[9] B. Bingöl, W. H. Meyer, M. Wagner, and G. Wegner, "Synthesis, microstructure, and acidity of poly(vinylphosphonic acid)," *Macromol. Rapid Commun.*, vol. 27, no. 20, pp. 1719–1724, 2006, doi: 10.1002/marc.200600513.

[10] B. Bingöl, C. Strandberg, A. Szabo, and G. Wegner, "Copolymers and hydrogels based on vinylphosphonic acid," *Macromolecules*, vol. 41, no. 8, pp. 2785–2790, 2008, doi: 10.1021/ma702807a.

[11] A. Yuchi, T. Sato, Y. Morimoto, H. Mizuno, and H. Wada, "Adsorption Mechanism of Trivalent Metal Ions on Chelating Resins Containing Iminodiacetic Acid Groups with Reference to Selectivity," *Anal. Chem.*, vol. 69, no. 15, pp. 2941–2944, 1997, doi: 10.1021/ac9612685.

[12] V. Najafi *et al.*, "Synthesis and characterization of alcogels based on ethylene glycol methyl ether methacrylate-vinyl phosphonic acid copolymers," *J. Polym. Res.*, vol. 19, no. 6, 2012, doi: 10.1007/s10965-012-9866-9.

[13] N. S. Kwak, H. M. Park, and T. S. Hwang, "Preparation of ion-exchangeable nanobeads using suspension polymerization and their sorption properties for indium in aqueous solution," *Chem. Eng. J.*, vol. 191, pp. 579–587, 2012, doi: 10.1016/j.cej.2012.03.018.

[14] N. S. Kwak, Y. Baek, and T. S. Hwang, "The synthesis of poly(vinylphosphonic acid-co-methacrylic acid) microbeads by suspension polymerization and the characterization of their indium adsorption properties," *J. Hazard. Mater.*, vol. 203–204, pp. 213–220, 2012, doi: 10.1016/j.jhazmat.2011.12.020.

[15] N. Sahiner, “Fast and high amount of uranyl ion uptake by p(vinyl phosphonic acid) microgels prepared by UV irradiation technique,” *Water. Air. Soil Pollut.*, vol. 225, no. 6, pp. 1–8, 2014, doi: 10.1007/s11270-014-1982-1.

[16] I. Anil, S. T. Gunday, A. Bozkurt, and O. Alagha, “Design of crosslinked hydrogels comprising poly(Vinylphosphonic acid) and bis[2-(methacryloyloxy)ethyl] phosphate as an efficient adsorbent for wastewater dye removal,” *Nanomaterials*, vol. 10, no. 1, 2020, doi: 10.3390/nano10010131.

[17] B. Onghena, E. Papagni, E. R. Souza, D. Banerjee, K. Binnemans, and T. Vander Hoogerstraete, “Speciation of lanthanide ions in the organic phase after extraction from nitrate media by basic extractants,” *RSC Adv.*, vol. 8, no. 56, pp. 32044–32054, 2018, doi: 10.1039/c8ra06712k.

[18] H. Haraguchi, A. Itoh, C. Kimata, and H. Miwa, “Speciation of yttrium and lanthanides in natural water by inductively coupled plasma mass spectrometry after preconcentration by ultrafiltration and with a chelating resin,” *Analyst*, vol. 123, no. 5, pp. 773–778, 1998, doi: 10.1039/a708253c.

[19] S. D. Alexandratos, D. R. Quillen, and W. J. Mcdowell, “Bifunctional Phosphinic Acid Resins for the Complexation of Lanthanides and Actinides,” *Sep. Sci. Technol.*, vol. 22, no. 2–3, pp. 983–995, 1987, doi: 10.1080/01496398708068994.

[20] J. Wang, “Adsorption of aqueous neodymium, europium, gadolinium, terbium, and yttrium ions onto nZVI-montmorillonite: kinetics, thermodynamic mechanism, and the influence of coexisting ions,” *Environ. Sci. Pollut. Res.*, vol. 25, no. 33, pp. 33521–33537, 2018, doi: 10.1007/s11356-018-3296-0.

[21] T. Kegl, A. Košak, A. Lobnik, and I. Ban, “Terbium ion adsorption from aqueous solution by using magneticγ-Fe2O3-NH4OH@SiO2 nanoparticles functionalized

with amino groups," *Materials (Basel).*, vol. 12, no. 8, 2019, doi: 10.3390/ma12081294.

[22] R. Arshady, "Suspension, emulsion, and dispersion polymerization: A methodological survey," *Colloid Polym. Sci.*, vol. 270, no. 8, pp. 717–732, 1992, doi: 10.1007/BF00776142.

[23] E. Vivaldo-Lima, P. E. Wood, A. E. Hamielec, and A. Penlidis, "An Updated Review on Suspension Polymerization," *Ind. Eng. Chem. Res.*, vol. 36, no. 4, pp. 939–965, 1997, doi: 10.1021/ie960361g.

[24] K. Kesenci and E. Piykin, "Production of poly [(ethylene glycol dimethacry1ate) -co- acrylamide] based hydrogel beads by suspension copolymerization," vol. 391, pp. 385–391, 1997.

[25] A. Tuncel, "Suspension polymerization of poly(ethylene glycol) methacrylate: A route for swellable spherical gel beads with controlled hydrophilicity and functionality," *Colloid Polym. Sci.*, vol. 278, no. 12, pp. 1126–1138, 2000, doi: 10.1007/s003960000317.

[26] L. MacArie and G. Ilia, "Poly(vinylphosphonic acid) and its derivatives," *Prog. Polym. Sci.*, vol. 35, no. 8, pp. 1078–1092, 2010, doi: 10.1016/j.progpolymsci.2010.04.001.

[27] X. Wang, X. Ding, Z. Zheng, X. Hu, X. Cheng, and Y. Peng, "Magnetic molecularly imprinted polymer particles synthesized by suspension polymerization in silicone oil," *Macromol. Rapid Commun.*, vol. 27, no. 14, pp. 1180–1184, 2006, doi: 10.1002/marc.200600211.

[28] G. I. Taylor, "The formation of emulsions in definable fields of flow," *Proc. R. Soc. London. Ser. A, Contain. Pap. a Math. Phys. Character*, vol. 146, no. 858, pp.

501–523, 1934, doi: 10.1098/rspa.1934.0169.

[29] P. J. Dowding and B. Vincent, “Suspension polymerisation to form polymer beads,” *Colloids Surfaces A Physicochem. Eng. Asp.*, vol. 161, no. 2, pp. 259–269, 2000, doi: 10.1016/S0927-7757(99)00375-1.

[30] S. Senel, H. Cicek, and A. Tuncel, “Production and Characterization of Poly (ethylene glycol dimethacrylate-styrene-glycidyl methacrylate) Microbeads,” *J. Appl. Polym. Sci.*, vol. 67, pp. 1319–1334, 1997.

[31] B. H. Stuart, *Infrared Spectroscopy: Fundamentals and Applications*. 2005.

[32] B. C. Melo, F. A. A. Paulino, V. A. Cardoso, A. G. B. Pereira, A. R. Fajardo, and F. H. A. Rodrigues, “Cellulose nanowhiskers improve the methylene blue adsorption capacity of chitosan-g-poly(acrylic acid) hydrogel,” *Carbohydr. Polym.*, vol. 181, no. October, pp. 358–367, 2018, doi: 10.1016/j.carbpol.2017.10.079.

[33] P. Dangelo *et al.*, “Revised ionic radii of lanthanoid(III) ions in aqueous solution,” *Inorg. Chem.*, vol. 50, no. 10, pp. 4572–4579, 2011, doi: 10.1021/ic200260r.

[34] C. Strandberg, C. Rosenauer, and G. Wegner, “Poly (vinyl phosphonic acid): Hydrodynamic properties and SEC-calibration in aqueous solution,” *Macromol. Rapid Commun.*, vol. 31, no. 4, pp. 374–379, 2010, doi: 10.1002/marc.200900605.

[35] D. Feng, B. Bai, H. Wang, and Y. Suo, “Novel Fabrication of PAA/PVA/Yeast Superabsorbent with Interpenetrating Polymer Network for pH-Dependent Selective Adsorption of Dyes,” *J. Polym. Environ.*, vol. 26, no. 2, pp. 567–588, 2018, doi: 10.1007/s10924-017-0972-y.

[36] A. Bashir, T. Manzoor, L. A. Malik, A. Qureashi, and A. H. Pandith, “Enhanced and Selective Adsorption of Zn(II), Pb(II), Cd(II), and Hg(II) Ions by a Dumbbell-And Flower-Shaped Potato Starch Phosphate Polymer: A Combined Experimental

and DFT Calculation Study," *ACS Omega*, vol. 5, no. 10, pp. 4853–4867, 2020, doi: 10.1021/acsomega.9b03607.

[37] E. A. Abdel-Galil, A. B. Ibrahim, and M. M. Abou-Mesalam, "Sorption behavior of some lanthanides on polyacrylamide stannic molybdophosphate as organic–inorganic composite," *Int. J. Ind. Chem.*, vol. 7, no. 3, pp. 231–240, 2016, doi: 10.1007/s40090-016-0080-1.

[38] S. Yngve, "Zur Theorie der sogenannten Adsorption EOD – Millions of books just a mouse click away ! In more than 10 European countries !," 1898.

[39] G. Ho, Y.S, McKay, "Pseudo-secon order model for sorption processes," *Process Biochem.*, vol. 34, no. 5, pp. 451–465, 199AD, doi: https://doi.org/10.1016/S0032-9592(98)00112-5.

[40] J. P. Simonin, "On the comparison of pseudo-first order and pseudo-second order rate laws in the modeling of adsorption kinetics," *Chem. Eng. J.*, vol. 300, pp. 254–263, 2016, doi: 10.1016/j.cej.2016.04.079.

[41] C. R. Lee, H. S. Kim, I. H. Jang, J. H. Im, and N. G. Park, "Pseudo first-order adsorption kinetics of N719 dye on TiO2 surface," *ACS Appl. Mater. Interfaces*, vol. 3, no. 6, pp. 1953–1957, 2011, doi: 10.1021/am2001696.

[42] "Coefficient-of-determination-R2 Di Bucchianico, .pdf." .

[43] E. D. Revellame, D. L. Fortela, W. Sharp, R. Hernandez, and M. E. Zappi, "Adsorption kinetic modeling using pseudo-first order and pseudo-second order rate laws: A review," *Clean. Eng. Technol.*, vol. 1, no. October, p. 100032, 2020, doi: 10.1016/j.clet.2020.100032.

[44] R.-S. Wu, Feng-Chin., Tseng, Ru-Ling., Juang, "KINETIC MODELING OF LIQUID-PHASE ADSORPTION OF REACTIVE DYES AND METAL IONS

ON CHITOSAN," *Water Res.*, vol. 35, no. 3, pp. 613–618, 2001, doi: https://doi.org/10.1016/S0043-1354(00)00307-9.

[45] J. Lin and L. Wang, "Comparison between linear and non-linear forms of pseudo-first-order and pseudo-second-order adsorption kinetic models for the removal of methylene blue by activated carbon," *Front. Environ. Sci. Eng. China*, vol. 3, no. 3, pp. 320–324, 2009, doi: 10.1007/s11783-009-0030-7.

[46] I. A. W. Tan, A. L. Ahmad, and B. H. Hameed, "Adsorption of basic dye on high-surface-area activated carbon prepared from coconut husk: Equilibrium, kinetic and thermodynamic studies," *J. Hazard. Mater.*, vol. 154, no. 1–3, pp. 337–346, 2008, doi: 10.1016/j.jhazmat.2007.10.031.

[47] Y. Xiao, J. Azaiez, and J. M. Hill, "Erroneous Application of Pseudo-Second-Order Adsorption Kinetics Model: Ignored Assumptions and Spurious Correlations," *Ind. Eng. Chem. Res.*, vol. 57, no. 7, pp. 2705–2709, 2018, doi: 10.1021/acs.iecr.7b04724.

[48] B. K. Aziz, D. M. S. Shwan, and S. Kaufhold, "Characterization of Tagaran natural clay and its efficiency for removal of cadmium (II) from Sulaymaniyah industrial zone sewage," *Environ. Sci. Pollut. Res.*, vol. 27, no. 31, pp. 38384–38396, 2020, doi: 10.1007/s11356-019-06995-x.

[49] F. Alakhras, "Kinetic Studies on the Removal of Some Lanthanide Ions from Aqueous Solutions Using Amidoxime-Hydroxamic Acid Polymer," *J. Anal. Methods Chem.*, vol. 2018, 2018, doi: 10.1155/2018/4058503.

[50] K. K. Swain, P. M. Mishra, and A. P. Devi, "Biosorption of praseodymium (III) using Terminalia arjuna bark powder in batch systems: Isotherm and kinetic studies," *Water Sci. Technol.*, vol. 77, no. 3, pp. 727–738, 2018, doi:

10.2166/wst.2017.589.

[51] G. Wójcik, “Sorption behaviors of light lanthanides(III) (La(III), Ce(III), Pr(III), Nd(III)) and Cr(III) using nitrolite,” *Materials (Basel).*, vol. 13, no. 10, 2020, doi: 10.3390/ma13102256.

[52] Y. Zhou, C. Yan, S. Zhou, T. Liang, and X. Wen, “Preparation of montmorillonite grafted polyacrylic acid composite and study on its adsorption properties of lanthanum ions from aqueous solution,” *Environ. Sci. Pollut. Res.*, vol. 26, no. 10, pp. 9861–9875, 2019, doi: 10.1007/s11356-019-04422-9.

[53] Q. Zhou, H. Yang, C. Yan, W. Luo, X. Li, and J. Zhao, “Synthesis of carboxylic acid functionalized diatomite with a micro-villous surface via UV-induced graft polymerization and its adsorption properties for Lanthanum(III) ions,” *Colloids Surfaces A Physicochem. Eng. Asp.*, vol. 501, pp. 9–16, 2016, doi: 10.1016/j.colsurfa.2016.04.030.

[54] X. Cao, Q. Wang, S. Wang, and R. Man, “Preparation of a novel polystyrene-poly(hydroxamic acid) copolymer and its adsorption properties for rare earth metal ions,” *Polymers (Basel).*, vol. 12, no. 9, 2020, doi: 10.3390/POLYM12091905.

[55] Z. S. Birungi and E. M. N. Chirwa, “The kinetics of uptake and recovery of lanthanum using freshwater algae as biosorbents: Comparative analysis,” *Bioresour. Technol.*, vol. 160, pp. 43–51, 2014, doi: 10.1016/j.biortech.2014.01.033.

[56] M. Wang, X. Li, W. Hua, L. Shen, X. Yu, and X. Wang, “Electrospun Poly(acrylic acid)/Silica Hydrogel Nanofibers Scaffold for Highly Efficient Adsorption of Lanthanide Ions and Its Photoluminescence Performance,” *ACS Appl. Mater. Interfaces*, vol. 8, no. 36, pp. 23995–24007, 2016, doi: 10.1021/acsami.6b08294.

[57] K. Dev, R. Pathak, and G. N. Rao, “Sorption behaviour of lanthanum(III), neodymium(III), terbium(III), thorium(IV) and uranium(VI) on amberlite XAD-4 resin functionalized with bicine ligands,” *Talanta*, vol. 48, no. 3, pp. 579–584, 1999, doi: 10.1016/S0039-9140(98)00274-4.

[58] H. Zhang, R. G. Mcdowell, L. R. Martin, and Y. Qiang, “Selective Extraction of Heavy and Light Lanthanides from Aqueous Solution by Advanced Magnetic Nanosorbents,” *ACS Appl. Mater. Interfaces*, vol. 8, no. 14, pp. 9523–9531, 2016, doi: 10.1021/acsami.6b01550.

[59] Y. Wei, K. A. M. Salih, M. F. Hamza, T. Fujita, E. Rodríguez-Castellón, and E. Guibal, “Synthesis of a new phosphonate-based sorbent and characterization of its interactions with lanthanum (Iii) and terbium (iii),” *Polymers (Basel).*, vol. 13, no. 9, 2021, doi: 10.3390/polym13091513.

[60] D. Baybaş and U. Ulusoy, “Polyacrylamide-clinoptilolite/Y-zeolite composites: Characterization and adsorptive features for terbium,” *J. Hazard. Mater.*, vol. 187, no. 1–3, pp. 241–249, 2011, doi: 10.1016/j.jhazmat.2011.01.014.

[61] M. M. Saeed and A. Rusheed, “Investigation of sorption of Tb(III) by 2-thenoyltrifluoroacetone supported onto polyurethane foam,” *Radiochim. Acta*, vol. 90, no. 1, pp. 35–42, 2002, doi: 10.1524/ract.2002.90.1_2002.35.

[62] C. Rill, Z. I. Kolar, G. Kickelbick, H. T. Wolterbeek, and J. A. Peters, “Kinetics and thermodynamics of adsorption on hydroxyapatite of the [160Tb]terbium complexes of the bone-targeting ligands DOTP and BPPED,” *Langmuir*, vol. 25, no. 4, pp. 2294–2301, 2009, doi: 10.1021/la803562e.

[63] M. R. Awual *et al.*, “Ligand field effect for Dysprosium(III) and Lutetium(III) adsorption and EXAFS coordination with novel composite nanomaterials,” *Chem.*

Eng. J., vol. 320, pp. 427–435, 2017, doi: 10.1016/j.cej.2017.03.075.

[64] Y. Hu, E. Drouin, D. Larivière, F. Kleitz, and F. G. Fontaine, "Highly Efficient and Selective Recovery of Rare Earth Elements Using Mesoporous Silica Functionalized by Preorganized Chelating Ligands," *ACS Appl. Mater. Interfaces*, vol. 9, no. 44, pp. 38584–38593, 2017, doi: 10.1021/acsami.7b12589.

[65] Q. Qu, Q. Gu, Z. Gu, Y. Shen, C. Wang, and X. Hu, "Efficient removal of heavy metal from aqueous solution by sulfonic acid functionalized nonporous silica microspheres," *Colloids Surfaces A Physicochem. Eng. Asp.*, vol. 415, pp. 41–46, 2012, doi: 10.1016/j.colsurfa.2012.08.059.

[66] F. Ge, M. M. Li, H. Ye, and B. X. Zhao, "Effective removal of heavy metal ions Cd 2+, Zn 2+, Pb 2+, Cu 2+ from aqueous solution by polymer-modified magnetic nanoparticles," *J. Hazard. Mater.*, vol. 211–212, pp. 366–372, 2012, doi: 10.1016/j.jhazmat.2011.12.013.

[67] F. An, B. Gao, X. Dai, M. Wang, and X. Wang, "Efficient removal of heavy metal ions from aqueous solution using salicylic acid type chelate adsorbent," *J. Hazard. Mater.*, vol. 192, no. 3, pp. 956–962, 2011, doi: 10.1016/j.jhazmat.2011.05.050.

[68] Y. Zhu, J. Hu, and J. Wang, "Competitive adsorption of Pb(II), Cu(II) and Zn(II) onto xanthate-modified magnetic chitosan," *J. Hazard. Mater.*, vol. 221–222, pp. 155–161, 2012, doi: 10.1016/j.jhazmat.2012.04.026.

3.6 List of figure

3.7 List of table

Chapter IV. Concluding remarks

This thesis has successfully conducted the heterogeneous polymerization methods, including O/W emulsion and W/O suspension polymerization methods, to prepare the polymeric spherical particles. These different polymerization methods produce particles having different size ranges.

In Chapter II, we successfully synthesized the phosphonic acid-functionalized styrene and divinylbenzene by O/W emulsion polymerization. Obtained particles are high uniformity, spherical with high monodisperse particle, and large specific surface area, confirmed by SEM images. Then, to evaluate the area and particle distribution, ImageJ software was used. Thus, Origin software was also used to calculate the diameter distribution of the particles. The overall calculation indicates that the polydispersity index (PDI) values are lower than 0.1. This result assumed that the obtained nanoparticles were monodisperse. Adsorption study for obtained polymer nanoparticles shows that there is no difference result between the presence and absence of phosphonic acid functional agent on the polymer surface. These findings were probably attributed to there are not having high enough VPA grafted onto PS-DVB nanoparticles. The effect of functional agents on adsorption capacity is unclear. Modification of the polymer surface using other phosphonic acid functional agents such as Diethyl Vinyl Benzyl Phosphonate (DEVBP) was also shown unsuccessful synthesis process.

In Chapter III, we successfully synthesized crosslinked poly(vinylphosphonic acid) particles by W/O suspension polymerization method using vinyl phosphonic acid (VPA) as monomer and poly(ethylene glycol) diacrylate (PEGDA) as a crosslinking agent. Several molar ratios of PEGDA were varied from 5% to 20% to produce various types of

particles, namely, PVPA-5, PVPA-10, PVPA-15, and PVPA-20. Polydisperse polymer particles were obtained through this method, as confirmed by an optical microscope with a size ranging from 10 – 200 μm; wrinkled surface morphology became apparent by increasing crosslinker concentration, as inferred from SEM images. In the preliminary adsorption study, PVPA-10 shown the highest adsorption capacity as compared to others. Thus, a batch adsorption experiment was conducted to study the adsorption behavior of trivalent (lanthanide series, Ln^{3+} = La^{3+}, Tb^{3+}, and Lu^{3+}) and divalent (Cu^{2+} and Zn^{2+}) metal ions onto PVPA-10 particles at the optimum condition. The kinetic adsorption parameters were evaluated using PFO and PSO kinetic models from the Lagergren equation. The adsorption kinetics was best described by either PFO or PSO kinetic model according to correlation coefficient (R^2) values, which is high enough for both kinetic models. However, the R^2 value does not guarantee the model acceptability. To avoid the spurious conclusion, the residues resulting from a linear fit kinetic model should be evaluated using other validation methods and exhibit how low the model error is. Model validation methods are used to determine the suitable kinetic model, including SSE, χ^2, MSE, RMSE, Δy (%), ARE, and SAE.

Consequently, the model that fits a datasheet would have R^2 closer to unity and lower values of the other validation methods. According to the assessment result of validation methods, PFO kinetic model is more appropriate and better to describe the adsorption kinetics of La^{3+}, Tb^{3+}, Lu^{3+}, Cu^{2+}, and Zn^{2+} ions onto PVPA-10 particles. It is recommended to always verify the assumption of a model and inspect the residual plot to determine the goodness of fit. Then, the adsorption isotherms were also investigated by applying Freundlich and Langmuir`s non-linear model. The maximum adsorption of La^{3+}, Tb^{3+}, Lu^{3+}, Cu^{2+}, and Zn^{2+} predicted using Langmuir adsorption isotherm model to be

0.185, 0.097, 0.088, 0.045, and 0.135 mmol g^{-1}, respectively.